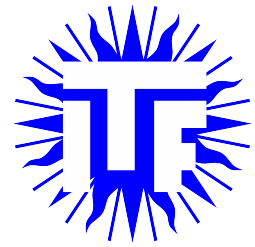




Utrecht University



GRADUATE SCHOOL OF NATURAL SCIENCES

On the construction and measurement of
conformal extensions of the Standard Model

Master thesis

D.J.W. Verweij

Theoretical Physics

Supervisor

dr. T. Prokopec

Institute for Theoretical Physics Utrecht

Second supervisor

dr. U. Gürsoy

Institute for Theoretical Physics Utrecht

June, 2019

*(...), it appears increasinlgy likely that dark matter
is not simple after all.*

– S. Furlanetto, 2019 [1]

But it never was!

– T. Prokopec, Journal Club discussion, 2019

Abstract

In this thesis, different conformal extensions of the Standard Model are studied. A general framework of quantum and thermal field theory is given to determine the effective potential up to one-loop order for general models. Also, it is found by studying symmetry-breaking patterns based on research from grand unified theories, that many models might have an strongly first-order electroweak phase transition, which can induce strong gravitational wave signals and baryogenesis. By determining multiple constraints on conformal extensions of the Standard Model from theoretical and experimental considerations, two new models are introduced: the adjoint $f\text{SU}(N)\text{cSM}$ and the $Mf\text{SU}(N)\text{cSM}$. For both the complete particle mass spectrum is calculated. Also, the already well-studied $\text{SU}(2)\text{cSM}$ is considered as a benchmark model for a numerical program, `CosmoTransitions`. The program is used to study the electroweak phase transition of the three models and for the $\text{SU}(2)\text{cSM}$ new results are found compared to previous work. For the two new models, unfortunately, no phase transition has been found, but a descriptive analysis is given for the temperature-dependence of their minima.

Acknowledgements

I would like to thank my supervisor, Dr. Tomislav Prokopec, for all the dedicated time to teach and instruct me on a weekly basis on this fascinating topic and all the aspects of writing and presenting an academic thesis. Also, my co-supervisor Dr. Bogumiła Świeżewska must be acknowledged, as she always was willing to clarify the underlying physics and helped me a lot with interpreting the numerical findings. It is safe to say that without the both of them, this thesis would not be in front of you. Furthermore, I would like to thank Marc Barroso Mancha for sifting out together all the aspects of CosmoTransitions.

I want to thank Daan Peerlings, Hendrik Snijder and Ruben Meijs for the more than welcome distractions from writing my thesis during the numerous lunch and coffee breaks. Also, I want to express my gratitude towards Koen Stemerink for extending his already long coffee breaks to include me. Lastly, I am grateful to my family for supporting me throughout this year and in particular my grandfather Jos, who probably will be one of the few who will read every word of this thesis.

Contents

Notation and convention	1
1 Introduction	3
2 Field theory tools for building conformal extensions of the SM	7
2.1 Quantum corrections to the effective potential	7
2.2 RSB through quantum loop corrections	8
2.2.1 RSB in massless scalar quantum electrodynamics	8
2.3 Thermal corrections to the effective potential	10
2.3.1 Thermal Field Theory	10
2.3.2 Daisy resummation	11
3 Theoretical and experimental constraints	15
3.1 Relativistic degrees of freedom	15
3.2 CP-violation and baryogenesis	15
3.3 Vacuum stability	16
3.4 Dark matter relic abundance	18
3.5 Higgs boson mass and VEV	18
3.6 LHC limits on heavy dark Higgs mass	18
3.7 Perturbativity	19
4 Examples of conformal extensions	21
4.1 Symmetry-breaking in general gauge groups	21
4.1.1 Symmetry breaking patterns in $SU(N)$ and $SO(N)$	22
4.1.2 Example of a symmetry breaking analysis	22
4.1.3 Resulting symmetry breaking patterns	24
4.1.4 Resulting particle behaviour of symmetry groups	24
4.2 The benchmark model: $SU(2)cSM$	25
4.2.1 Mass eigenvalues of $SU(2)cSM$	25
4.3 The adjoint $fSU(N)cSM$	26
4.3.1 Mass eigenvalues	27
4.3.2 Eigenvalues in large- N limit	28
4.3.3 Eigenvalues for $N = 2$: the adjoint $fSU(2)cSM$	29
4.3.4 Thermal masses of the adjoint $fSU(N)cSM$	31
4.4 The $MfSU(N)cSM$	31
4.4.1 Mass eigenvalues	32
5 The electroweak phase transition	35
5.1 Theoretical framework of bubble nucleation	35
5.1.1 Nucleation Temperature T_n	37
5.1.2 Percolation temperature T_p	38
5.1.3 Reheating temperature T_r	40
5.2 Bubble hydrodynamics	40
5.2.1 Bubble collisions	41
5.2.2 Soundwaves	42
5.2.3 Turbulence	42

6	Numerical analysis	45
6.1	The over- and undershoot method	45
6.2	Result for the benchmark model SU(2)cSM	46
6.2.1	Results on benchmark points	47
6.2.2	Figures of benchmark point 7	48
6.2.3	The SGWB of the SU(2)cSM	50
6.3	Analysis of the adjoint fSU(2)cSM and MfSU(2)cSM	50
7	Conclusion	55
A	Full Lagrangian of the conformal extensions	57
A.1	Lagrangian of the adjoint fSU(N)cSM	57
A.2	Lagrangian of the MfSU(N)cSM	58
A.3	Thermal corrections to the Standard Model and the SU(2)cSM	58
B	HTL calculation of the scalar self-energy	60
C	Explicit expressions for the symmetry breaking analysis	62

Notation and conventions

Unless mentioned otherwise, the following notation and conventions are used throughout this thesis:

- All equations are in natural units to improve their readability:

$$c = \hbar = k_B = 1 \tag{1}$$

- For renormalization procedures, the \overline{MS} -scheme is used. Furthermore, any divergent integrals are solved by dimensional regularization.
- Gauge freedom is fixed by working in Landau gauge. This means no ghosts have to be taken into account.

For readability purposes, many recurring terms are abbreviated after their first appearance in this thesis. Here an overview of all abbreviations used throughout this thesis are given:

- adjoint fSU(N)cSM: Conformal extension of the Standard Model with a $SU(N)$ gauge group, a scalar under the adjoint representation of this gauge group and Dirac fermions, as defined in Section 4.3
- BSM: Beyond the Standard Model physics
- CKW-matrix: Cabibbo-Kobayashi-Maskawa matrix
- CMB: Cosmic Microwave Background
- CP: Charge Parity
- CW-mechanism: Coleman-Weinberg mechanism
- EWPT: Electroweak Phase Transition
- GUT: Grand Unified Theory
- HTL: Hard Thermal Loop
- IR/UV: Infrared and Ultraviolet
- ITF: Imaginary Time Formalism
- LISA: Laser Interferometer Space Antenna
- MfSU(N)cSM: Conformal extension of the Standard Model with Majorana fermions and a $SU(N)$ gauge group, as defined in Section 4.4
- RSB: Radiative Symmetry breaking
- RTF: Real Time Formalism
- SNR: Signal-to-Noise Ratio
- SGWB: Stochastic Gravitational Wave Background

- (c)SM: (Conformal) Standard Model
- SSB: Spontaneous Symmetry Breaking
- TFT: Thermal Field Theory
- VEV: Vacuum Expectation Value

As a last remark, this thesis is written at the level of second-year master students. Therefore a general understanding of quantum field theory is assumed, as well as a basic knowledge of cosmology.

Chapter 1

Introduction

With the experimental measurement of the Higgs boson in 2012 [2–4], the complete particle zoo of the Standard Model (SM) has been found. The Higgs boson gives all the other SM particles their masses through spontaneous symmetry breaking (SSB) via the Brout-Englert-Higgs mechanism [5, 6]. This means there are no free parameters in the SM, except for the Higgs mass $m_h = 125.06$ GeV and its vacuum expectation value $v = 246$ GeV. Yet this raises the question why these parameters exactly have these values? Is there some underlying process, which sets the energy scales, or is there perhaps something special with this particular energy scale? The SM is not able to provide any answers, as all predicted particles are found and all experiments agree perfectly with the SM predictions. So one is naturally urged to look beyond the SM, towards new physics, in search of answers.

Perhaps the most intriguing mystery in the SM is the hierarchy problem. It states that it is extremely unlikely that the Higgs mass is as light as it is under influence of quantum corrections. Since the SM is ultra-violet (UV) complete and renormalizable, it can be valid to very high energies. So no new physics is needed up to the Planck scale ($\sim 10^{18}$ GeV), but it is hard to believe that up to this scale the Higgs' bare mass exactly cancels the quantum corrections, both of order 10^{18} GeV, up to a factor of ~ 100 GeV. One could compare this to putting an ice cube in the oven and expecting that the 10^{20} hot air particles exactly bounce off each other in such a way, that they do not impart thermal energy on the ice cube, leaving it frozen. This 'fine-tuning' seems unnatural and therefore one would like to change the SM in such a way that there is no need for it.

By getting rid of the bare mass altogether by making the SM conformally invariant (i.e. no preferred mass scales in the Lagrangian), one clears the need for fine-tuning and protects the Higgs mass from quantum corrections [7]. For this, one needs a mechanism to dynamically generate the required mass scale of the Higgs boson. Currently, there are two main fields of interest to provide this mechanism. First of all, supersymmetry breaking could generate a mass scale by introducing supersymmetric partners to all the SM particles. However, experiments, including the measurement of the Higgs mass, have severely constrained supersymmetric models [8]. The second mechanism that could account for the generation of the Higgs mass scale is radiative symmetry breaking (RSB) [9]. Conformal models can produce mass scales radiatively through inclusion of higher-order quantum-loop corrections, which break the symmetry of a conformal model.

The most minimalistic conformal model is the conformal SM (cSM) [7, 9]. The cSM could generate the Higgs mass via RSB and hence no fine-tuning is needed. However, this is only possible for a large self-coupling of the Higgs field, which in turn leads to troublesome Landau poles below the Planck scale for the running coupling constant of the top quark [10, 11]. So what is needed are conformal extensions of the SM, which can generate all known SM masses, but do not produce Landau poles. Multiple models have been proposed in recent years: extending the SM with a real or complex scalar [12, 13],

multiple scalars [14], gauge groups [10, 15–18] and fermions [14, 19, 20]. These models can also potentially solve other problems, such as dark matter, neutrino masses and baryogenesis. How conformal extensions can address these problems, will be discussed in Chapter 3.

If one would extend the cSM to include more particles in the electroweak sector (i.e. coupled to the Higgs boson, but 'hidden' from the rest of the SM), RSB becomes possible. The natural question to ask next is when this radiative symmetry-breaking has taken place. Kirzhnits [21, 22] was the first to recognize that symmetry restoration of the electroweak theory must have taken place in the early Universe for high enough temperatures. The electroweak phase transition (EWPT) from the symmetric phase, where the Higgs VEV $\langle h \rangle = 0$, to the broken phase with $\langle h \rangle \neq 0$, must have happened at temperatures of the order of the electroweak scale ~ 100 GeV. The interesting property of conformal extensions is that the EWPT is generally a very strong first-order phase transition (see Chapter 5), which could be a source of baryogenesis [23].

Besides baryogenesis, first-order phase transitions can also source gravitational wave. At the critical temperature T_c these phase transitions have the symmetry-breaking and symmetric minima coexisting as degenerate minima. When the Universe cools down further, the symmetry-breaking minimum will become the global minimum, but the system can be captured in the symmetric state (false vacuum) due to a barrier between the two. Through quantum or thermal fluctuations the system can tunnel to the true vacuum through the barrier. As these fluctuations have a statistical nature, not everywhere in the false vacuum this tunneling will happen at the same time. Bubbles of true vacuum will form and expand into the false vacuum, ultimately taking over the whole Universe. Collisions of these bubbles are very energetic processes, as they contain the potential energy between the true and false vacuum. This energy is transferred into heat and, more interestingly, gravitational energy. The gravitational energy is radiated away in the form of gravitational waves. As gravitational waves are not hindered by anything in spacetime, they will propagate through the whole Universe, creating a gravitational wave background.

This leads to another incentive to study conformal extensions. Since a few years, it is experimentally possible to measure gravitational waves directly with the LIGO-detector. Unfortunately, the peak sensitivity frequency range of LIGO is several orders of magnitude larger than the expected signal from an electroweak phase transition in the early Universe, which is of the order of mHz. Future detectors are being constructed and the most promising one is the Laser Interferometer Space Antenna (LISA) [24]. LISA is a space-based gravitational wave detector in free-fall around the Sun, which measures deformations of space-time by observing interferometry of laser signals sent through space over a distance of 2.5 million kilometers. This makes it sensitive in the same frequency range as the expected gravitational wave signals from phase transitions in the early Universe [25–27].

The technological feasibility of LISA has already been demonstrated by LISA Pathfinder, a smaller test version launched in 2015. LISA Pathfinder exceeded all expectations, as it was originally designed to have a strain sensitivity an order of magnitude smaller than that from LISA, but has exceeded the requirements for LISA on the entire frequency band of LISA. These findings along with the first direct measurements of gravitational waves have induced a renewed interest in conformal extensions, as they could be experimentally measurable by LISA, which is scheduled to launch in 2034.

As it stands, conformal extensions are a very promising field of research for both theoretical and experimental reasons. However, if one wants to measure in 2034, which, if any, conformal extension is the one that correctly describes nature, more knowledge is needed on the signatures of different conformal extensions. Do they depend on the particle spectrum of the model? And is there a way to discriminate between different models? Are all extensions physically possible and can they solve other open questions in physics, such as dark matter or baryogenesis?

In this thesis, a general attempt is made to analyze how conformal extensions can behave. For this, first a solid theoretical groundwork of quantum and thermal field theory will be given in Chapter 2. Next, in Chapter 3, theoretical and experimental constraints on the particle spectra that might arise, are considered. Then in Chapter 4, three models are introduced. First, the $SU(2)cSM$, which has been studied by preceding master theses in the same Cosmology group[28, 29], is introduced as a benchmark model for numerical calculations. Then two new models are introduced, based on the considerations of the previous two chapters, namely the adjoint $fSU(N)cSM$ and the $MfSU(N)cSM$. These models are analyzed in Chapter 6 with the numerical program `CosmosTransitions` [30], which had not been used on conformal extensions yet. To better analyze these models, first in Chapter 5 the EWPT and bubble nucleation is discussed in more technical detail.

Chapter 2

Field theory tools for building conformal extensions of the SM

The electroweak phase transition is described by its order parameter, the vacuum expectation value (VEV) of the scalar field. In order to describe the dynamics of the VEV, one can treat it as a classical field and write down a classical potential. This potential can be improved by including quantum effects up to a certain loop order. As the phase transition must have taken place at high temperatures in the early Universe, thermal effects must also be taken into account. The effective potential contributions for quantum corrections are discussed in Section 2.1. Then it is explained how RSB can occur through these quantum corrections in Section 2.2. For a discussion of the thermal corrections, a theoretical introduction to Thermal Field Theory is given and the general one-loop thermal corrections are given in Section 2.3.

2.1 Quantum corrections to the effective potential

To see how RSB can occur in a symmetric theory, first the effective one-loop potential is needed. RSB can happen solely due to quantum fluctuations, so these are considered first. The thermal fluctuations make the symmetry-breaking temperature dependent. Calculation of quantum corrections to the effective potential can be done with the method of the Effective action [31]. This has been done in detail in previous master theses [28, 29], so here only a heuristic treatment is given. By varying the action and only considering terms which are up to quadratic in the fluctuations, one can find the quantum one-loop corrections.

$$V_{\text{eff}}^{(1)}(\phi) = \frac{i}{2} \int \frac{d^d k}{(2\pi)^d} \text{Tr} \log \Delta^{-1}(\phi; k) \quad (2.1)$$

here $\Delta^{-1}(\phi; k)$ is the inverse propagator, which depends on the particle species, which can be scalars, fermions or gauge bosons. By using the \overline{MS} -scheme to renormalize the theory and working in Landau gauge, this can also be written as in Equation (2.2). The result is generally given for all species of particles. For the complete derivation of the effective potential using path-integral formalism for the different particle types, see [32].

$$V^{(1)}(\phi) = \frac{1}{64\pi^2} \sum_a \xi_a m_a^4(\phi) \left(\log \frac{m_a^2(\phi)}{\mu^2} - \chi_a \right) \quad (2.2)$$

$$\xi_a = \begin{cases} 1 & \text{scalars} \\ -4 & \text{Dirac fermions} \\ -2 & \text{Majorana fermions} \\ 3 & \text{vector bosons} \end{cases} \quad \chi_a = \begin{cases} \frac{3}{2} & \text{scalars + Dirac/Majorana fermions} \\ \frac{5}{6} & \text{vector bosons} \end{cases} \quad (2.3)$$

The constant ξ_a comes from the degrees of freedom of the particle species and the minus sign from the fact that fermionic fields are treated as Grassmann variables. The second constant χ_a is dependent on the renormalization scheme and accounts for the counterterms needed to renormalize the theory. The mass terms m_a^2 are the tree-level field-dependent mass eigenvalues of the mass matrix M^2 , which appears in the propagator:

$$\Delta^{-1} = k^2 + M^2 \quad (2.4)$$

The mass matrix consists of mass terms from perturbative corrections to the propagator and from tree-level mass terms in the Lagrangian. The latter is in this thesis not possible, as classically conformal models do not have dimensionful (and thus mass) terms in the tree-level potential. The perturbative corrections are discussed in more detail in Section 2.3.2 for the thermal corrections and in the next section for the quantum corrections.

2.2 RSB through quantum loop corrections

In models which have a classical scale symmetry (i.e. no tree-level mass terms), mass scales can still dynamically be generated by quantum higher-order loop corrections through radiative symmetry breaking or the Coleman-Weinberg mechanism (CW-mechanism) [9]. The advantage of the CW-mechanism is that one does not have to manually insert a mass, which is in line with the naturalness most theoretical physicists aim for [7]. The symmetry gets broken by quantum loop effects and the scalar condenses to its VEV. So this is not the same as, but definitely related to, the Brout-Englert-Higgs mechanism [5, 6], which explains how the SM gauge bosons get their mass via EWSB [33–35]. Radiative symmetry breaking can thus be used in extensions of the SM to account for the VEV and mass of the SM-Higgs.

As there is no better way to explain RSB than by an example, massless scalar quantum electrodynamics is considered just as in the original paper by Coleman and Weinberg. [9]¹ It will show how a tree-level conformal theory can symmetry-break to a preferred mass-scale by radiative corrections.

2.2.1 RSB in massless scalar quantum electrodynamics

Perhaps the most simple theory which has radiative symmetry breaking, is massless scalar quantum electrodynamics with a complex scalar field $\phi = \phi_1 + i\phi_2$ coupled to $U(1)$ electromagnetism with coupling constant e . The bare mass of the scalar is set to zero to give the Lagrangian:

$$\mathcal{L} = -\frac{1}{4}F_{\mu\nu}^2 + \frac{1}{2}|D_\mu\phi|^2 - \frac{\lambda}{4!}|\phi|^4 + \text{counterterms} \quad (2.5)$$

It can be easily seen that the minimum of the potential $V \sim |\phi|^4$ is at $(\phi_1, \phi_2) = (0, 0)$. Now one can start to include quantum loop-corrections to compute the effective potential V_{eff} . Up to one-loop, one has first the tree-level diagram with four external ϕ 's and then one-loop diagrams with internal ϕ_1, ϕ_2 and photon loops and $2n$ external scalar lines.

This yields the following effective potential with the terms in order of how they were mentioned in the previous sentence as a function of the classical field ϕ_c :

$$V_{\text{eff}} = \frac{\lambda}{4!}\phi_c^4 + I\left(\frac{1}{2}\lambda\phi_c^2\right) + I\left(\frac{1}{6}\lambda\phi_c^2\right) + 3I(e^2\phi_c^2) - \frac{1}{2}C_1\phi_c^2 - \frac{1}{4!}C_2\phi_c^4 \quad (2.6)$$

Here $I(x^2)$ is a standard integral, which arises naturally from considering n -point functions [31]. It can be solved using a Wick rotation and a cutoff term Λ :

¹They also consider massless ϕ^4 -theory. However, as they also note, this theory only has symmetry-breaking as an artefact of the perturbative expansion. Higher-order expansions would erase the minimum.

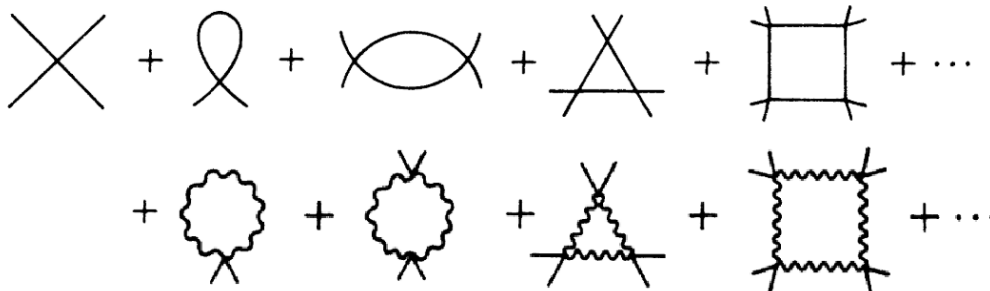


Figure 2.1: All the relevant diagrams for up to one-loop quantum corrections of the effective potential. The first line has the tree-level interaction and loop-diagrams with scalar-loops. The second line shows the same for loop-diagrams with photon-loops. All scalar lines can represent either ϕ_1 or ϕ_2 . Picture adjusted from [36].

$$\begin{aligned}
 I(x^2) &= i \int \frac{d^4k}{(2\pi)^4} \sum_{n=1}^{\infty} \frac{1}{2n} \left(\frac{x^2}{k^2 + i\epsilon} \right)^n \\
 &= -\frac{i}{2} \int \frac{d^4k}{(2\pi)^4} \ln \left(1 - \frac{x^2}{k^2 + i\epsilon} \right) \\
 &= \frac{x^2 \Lambda^2}{32\pi^2} + \frac{x^4}{64\pi^2} \left(\ln \frac{x^2}{\Lambda^2} - \frac{1}{2} \right)
 \end{aligned} \tag{2.7}$$

This is similar to Equation (2.1), which is what one would expect. The expression is still logarithmically and quadratic divergent. So to cancel the divergences, the counterterm constants C_1 and C_2 are fixed. By requiring that the second derivative of V_{eff} must be zero for some value $\phi_c = M$, C_1 is fixed. Similarly, one can require that:

$$\left. \frac{d^4 V_{\text{eff}}}{d\phi_c^4} \right|_{\phi_c=M} = \lambda \tag{2.8}$$

Fixing C_1 and C_2 in this way, will cancel the divergent terms from the integrals $I(x)$ for almost all values of M . However, the value $M = 0$ would lead to an IR-divergence due to the logarithmic term. So one needs to choose an arbitrary mass scale $\phi_c = M$, as there is no natural mass scale in this model. In conclusion, starting from a conformal model without any preferred mass scales, due to quantum loop-corrections one will end up with a mass scale in the theory. The precise value of this scale is just a matter of choice as one can reparametrize the coupling constant λ , which is just the renormalization group².

If one now chooses $M = \langle \phi \rangle$ with $\langle \phi \rangle$ the minimum of the effective potential, the following effective potential is found after rewriting it using renormalization conditions:

$$V_{\text{eff}} = \frac{3e^4}{64\pi^2} \phi_c^4 \left(\ln \frac{\phi_c^2}{\langle \phi \rangle^2} - \frac{1}{2} \right) \tag{2.9}$$

V_{eff} is plotted along with the tree-level potential in Figure 2.2. This example thus clearly illustrates the way RSB can take place, but it is not the full story. It is also possible to calculate one-loop corrections from thermal fluctuations via thermal field theory. These corrections can induce symmetry breaking at high enough temperatures by introducing a mass dependence on temperature, which would imply a phase transition. So the corrections discussed in this section form the zero-temperature effective potential (along with the tree-level potential), whereas the next section will discuss the finite-temperature effective potential.

²So no real new dimensionful parameter is added, it should be viewed more like defining the unit of mass, which is called dimensional transmutation.

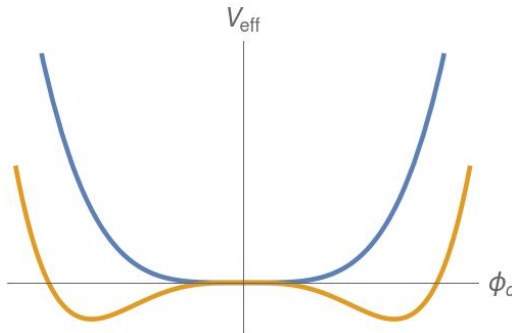


Figure 2.2: Plot of the tree-level potential (blue) and the effective potential V_{eff} (orange). It is clear that symmetry breaking takes place and the minimum changed from $\phi_c = 0$ to $\phi_c = \langle\phi\rangle$. Both potentials have been rescaled in order to exemplify the symmetry breaking.

2.3 Thermal corrections to the effective potential

Already in 1972, it was found that spontaneously broken symmetries can be restored at high temperatures [21]. This means that if one wants to study symmetry breaking in the early Universe, one can not use the standard quantum field theory, which is valid in the vacuum, but one needs a modification in the presence of a thermal bath. The field theory of interest for this is thermal field theory (TFT).³

2.3.1 Thermal Field Theory

TFT is used to describe large sets of interacting particles in a thermodynamical environment. These interactions include non-Abelian gauge theories, which are present in the SM and possibly in extensions of the SM. As has been mentioned, quantum field theories can exhibit phase transitions and TFT is the tool to describe them. TFT uses the standard path-integral formalism, but includes temperature as a complex time variable in the Boltzmann factor ($t = i\tau = -i\beta = -i/T$) via a Wick rotation. The resulting integral over time can be solved with two different formalisms.

The first formalism is the imaginary-time formalism (ITF), first introduced by Matsubara [45], which sums over the Matsubara frequencies from the Fourier transform. All fields now become functions of imaginary time. The advantage of this formalism is that one can use the known Feynman rules with only slight modifications. The disadvantage is that observables, which are real time, can only be computed by doing an analytical continuation to the real time axis.

The other approach is real-time formalism (RTF), where one solves the integral by choosing a contour in the complex plane and use contour integration. This yields everything directly in real time, but introduces 2×2 -matrices as propagators, making the Feynmann rules more complicated. In this thesis, ITF is used to find the thermal contributions to the effective potential, as these require the calculations of multiple Feynmann diagrams.

Just as for the zero-temperature effective potential, one-loop thermal corrections can be found by varying the action. This is the same quantity as in Equation (2.1):

$$V^{(1)}(\phi) = \frac{1}{2(2\pi)^4} \int d^4\mathbf{k} \log[\mathbf{k}^2 + m^2(\phi)] \quad (2.10)$$

Here $\mathbf{k} = (\vec{k}, k_4)$ is the four-momentum in the loop. The integral over imaginary time is now rewritten into a sum over Matsubara frequencies ($\omega_n = 2\pi nT$ for bosons and

³For further reading, one can turn for a general discussion to [37–39] and a discussion in the context of phase transitions (in the early Universe) to [23, 40–44]

$\omega_n = (2n + 1)\pi T$ for fermions).

$$\int \frac{dk_4}{2\pi} f(k_4) \rightarrow T \sum_{n=-\infty}^{\infty} f(k_4 = i\omega_n) \quad (2.11)$$

The integral is now split into a zero-temperature and finite-temperature contribution. The zero-temperature contribution is already discussed in the previous section. The sum over Matsubara frequencies can be evaluated by replacing it with a standard contour integral and then solving both the contour integral and the angular coordinates, leaving the integration over the radial component of the momentum k . Here the radial momentum is rescaled to $k \rightarrow k/T$, which yields an extra factor of T^3 :

$$V_T^{(1)}(\phi) = \frac{T^4}{2\pi^2} \int_0^\infty dk k^2 \log[1 - e^{-\sqrt{k^2 + m^2(\phi)}/T}] \quad (2.12)$$

Generalizing this to different types of particles and introducing the notation $J_{B,F}$ for the thermal functions, the thermal part of the effective one-loop potential becomes:

$$V_T^{(1)}(\phi) = \frac{T^4}{2\pi^2} \sum_a n_a J_a \left(\frac{m_a^2(\phi)}{T^2} \right) \quad (2.13)$$

where the thermal functions are defined as:

$$J_{B/F}(y^2) = \int_0^\infty dx x^2 \log[1 \mp e^{-\sqrt{x^2 + y^2}}] \quad (2.14)$$

Common expansions for the thermal functions J_B and J_F are the high-temperature limit ($m(\phi)/T \ll 1$), which can be analytically computed:

$$\begin{aligned} J_B(y^2) &= -\frac{\pi^4}{45} + \frac{\pi^2}{12}y^2 - \frac{\pi}{6}y^3 - \frac{1}{32}y^4 \log \frac{y^2}{a_B} \\ &\quad - 2\pi^{7/8} \sum_{m=1}^{\infty} (-1)^m \frac{\zeta(2m+1)}{(m+2)!} \Gamma(m+1/2) \left(\frac{y^2}{4\pi^2} \right)^{m+2} \end{aligned} \quad (2.15)$$

$$\begin{aligned} J_F(y^2) &= \frac{7\pi^4}{360} - \frac{\pi^2}{24}y^2 - \frac{1}{32}y^4 \log \frac{y^2}{a_F} \\ &\quad - \frac{\pi^{7/2}}{4} \sum_{l=1}^{\infty} (-1)^l \frac{\zeta(2l+1)}{(l+1)!} (1 - 2^{-2l-1}) \Gamma(l+1/2) \left(\frac{y^2}{\pi^2} \right)^{l+2} \end{aligned} \quad (2.16)$$

$$\text{where } a_B = 16a_F = 16\pi^2 e^{3/2 - 2\gamma_E}$$

From the bosonic thermal function, one can already see that for high temperatures, there will be a cubic contribution to the potential. This is important, since a cubic term can generate a barrier between two minima, which results in a first-order phase transition. For certain values of the scalar fields, it is possible that there are imaginary terms in the effective potential, due to this cubic term. This has a physical meaning, as the imaginary terms indicate a physical instability in the model. The imaginary part of the effective potential indicates thus that the system is not in a thermal equilibrium and that one should not use the one-loop approximation, but the full non-equilibrium formalism [46]. Combining Equations (2.2) and (2.13) now yields all the one-loop corrections to the effective potential.

2.3.2 Daisy resummation

For the thermal part the one-loop expansion is not the complete story as was already recognized directly during the first papers on the effective thermal potential [22, 47]. Perturbativity breaks down for high temperatures, where higher order loops contribute as much as or more as the tree-level and one-loop terms, due to infrared (IR) divergences (the zero-momentum modes ω_0). As fermions do not have zero frequency modes

($\omega_n = (2n + 1)\pi T \neq 0 \forall n$), they do not suffer from these IR divergences. For high temperatures, the IR-divergent diagrams need to be resummed. This procedure is called Daisy resummation, since the problematic divergent diagrams are of the (super)Daisy class (see Figure 2.3).

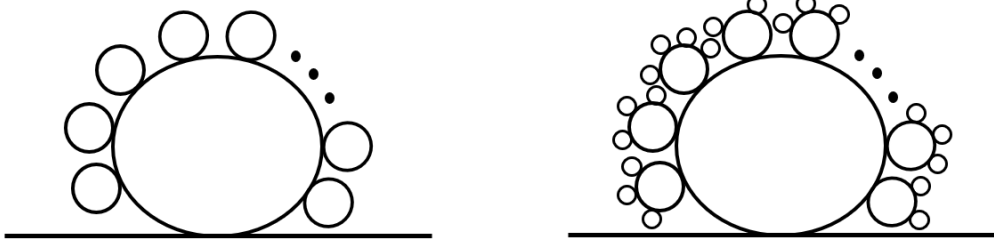


Figure 2.3: Schematic representation of the Feynman diagrams belonging to the daisy (left) and superdaisy (right) class. The name originates from their similarity to the daisy flower. Originally, these diagrams were first named ring diagrams [36].

The Daisy resummation can be done in two ways. Both rely on calculating the one-loop self energy $\Pi(m^2(\phi), T)$ at finite energy in the infrared limit, which is given by:⁴

$$\Pi(m^2(\phi), T) = \frac{\partial^2}{\partial \phi^2} \left(V^{(0)}(\phi) + V^{(1)}(m^2(\phi)) + V_T^{(1)}(m^2(\phi), T) \right) \quad (2.17)$$

The main difference between the two methods is how to implement the resummed propagator as a mass correction back into the effective potential:

$$\Delta_{\text{resum}}(\phi, T) = \frac{1}{P^2 - \Pi(m^2(\phi), T)} \quad (2.18)$$

The Arnold-Espinosa method

Historically, the first method to calculate the Daisy correction is the Arnold-Espinosa method [41]. This method consists in replacing the mass $m^2(\phi)$ by an effective mass $\bar{m}^2(\phi, T)$, which is now also dependent on temperature T via the self-energy Π :

$$\bar{m}^2(\phi, T) = m^2(\phi) + \Pi(m^2(\phi), T) \quad (2.19)$$

This replacement must only be done at the level of the m^3 -terms in the high-temperature expansions as given in Equation (2.15). These terms namely originate from zero-frequency- (ω_0 -)modes, which are the cause of the IR-divergences [43].⁵ One can calculate this through and ends up with effectively adding an extra term $V_{\text{daisy}}^{(1)}$ to the effective potential:

$$V_{\text{daisy}}^{(1)}(\phi, T) = -\frac{T}{12\pi} [\bar{m}^3(\phi, T) - m^3(\phi)] \quad (2.20)$$

However, the validity of this method was quickly questioned [48] for higher-order corrections and more complicated theories, which included non-Abelian gauge symmetries.

Parwani method

The second method is the Parwani method [49], which will be used in this thesis. It determines thermal contributions from the pole of the effective gauge or scalar propagator $1/(P^2 - \Pi(p^0, \vec{p}))$ ⁶. The induced thermal mass is then equal to the real part of this pole at zero momentum:

⁴In this case, taking the infrared limit corresponds to calculating the self-energy at zero external momentum, which is calculated by taking the second derivative of the one-loop effective potential.

⁵The IR-divergence comes from zero-momentum in the loops for zero-frequency modes

⁶Here $P^\mu = (p^0, \vec{p})$ is the external 4-momentum

$$m_{\text{thermal}}^2 = \Pi_0 \quad (2.21)$$

so that $m_{\text{eff}}^2 = m^2 + m_{\text{thermal}}^2$. The effective mass is then swapped in for all mass terms in the effective potential (Equations (2.2) and (2.13)). The thermal self-energy also ensures the renormalizability of the thermal effective potential as the resummed propagator in Equation (2.18) is only UV-divergent at zero temperature, which is already handled by the counterterms of the zero-temperature effective potential.

Thermal self-energy

Now the last, but definitely not least, step is to actually determine the self-energy. Calculating the self-energy up to any order is in ITF similar to the standard perturbative approach for self-energy in quantum field theory of $T = 0$. However, now one has to identify all diagrams with IR divergences that contribute to the propagator.

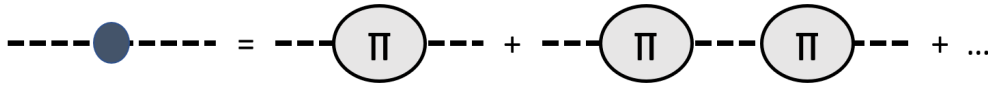


Figure 2.4: The resummed scalar propagator in terms of higher-order self-energy corrections.

These diagrams will have vertices where all corresponding momenta are soft, which requires a resummation and inclusion of an effective vertex and propagator. This is called the hard thermal loop effective theory (HTL effective theory), which seems counterintuitive. The name comes from the assumption that the loop momenta of the resummed diagrams are hard, otherwise perturbativity will still break down. As only one-loop is considered, the resummed vertex is not needed in this thesis and one only needs to focus on the propagator. Vertices will have always one or more hard momenta from the resummed propagators.

A general discussion of calculating scalar, gauge boson and fermion propagators can be found in [50]. However, for this thesis only the self-energy is needed to one-loop. In general, the one-loop self-energies can now be calculated using ITF for scalars and gauge bosons. The self-energies will depend on the model as a fermion loop will give a different contribution than a scalar loop. To explicitly calculate all possibilities has no higher purpose for this thesis, so only the general final contributions from loops to the self-energy are given here. The explicit calculations for the scalar self-energy are given in Appendix B and the one for the gauge bosons can be found in [42].

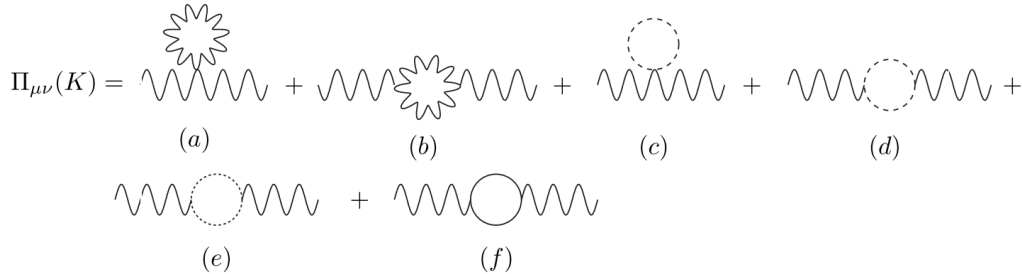


Figure 2.5: The six contributing one-loop diagrams to the gauge propagator. First, the 3- and 4-point gauge-interactions in (a) and (b). Three contributions from scalar loops in (c), (d) and (e), where the latter is a ghost-loop. Lastly, a fermion-loop in (f). Picture taken from [42].

All possible one-loop diagrams contributing to the scalar self-energy are given in Figure B.1. They lead to the following general formula for the thermal mass of a scalar

field:

$$m_{s, \text{thermal}}^2 = \frac{6\lambda + 3g^2 C_2(r_s) + N_c \lambda_f^2}{12} T^2 \quad (2.22)$$

where λ is the self-coupling constant of the scalar field, g the coupling to the gauge bosons, $C_2(r_s)$ the quadratic Casimir invariant for the representation r_s of the scalar field and finally N_c the number of colours of the fermion with coupling λ_f . Note that in models with more than one scalar, not only self-interactions must be taken into account, but also interactions between the scalars. This is just recounting possible Wick contractions and adding a similar term to Equation (2.22). For the gauge boson self-energy $\Pi_{\mu\nu}$ with gauge coupling g , one can draw six different possible one-loop Feynmann diagrams as shown in Figure 2.5. Diagrams (a),(b) and (e)⁷ yield a term proportional to the quadratic Casimir invariant $C_2(r_{GB})$, where now r_{GB} is the representation of the gauge bosons. The quadratic Casimir invariant depends on the gauge group and the representation and is for a general $SU(N)$ gauge group given by:

$$C_2(r) = \begin{cases} \frac{N^2 - 1}{2N} & r = \text{fundamental representation} \\ N & r = \text{adjoint representation} \end{cases} \quad (2.23)$$

The scalar-loop diagrams (c) and (d) depend on the number of scalars N_s and likewise the fermion-loop diagram (f) depends on the number of fermions N_f ⁸. Together they yield:

$$m_{\text{GB, thermal}}^2 = \frac{g^2 T^2}{6} \left(2C_2(r_{GB}) + \frac{N_f}{2} + \frac{N_s}{4} \right) \quad (2.24)$$

where a factor of two is added for the gauge boson contributions, compared to [42].⁹ Note that in the IR-limit, transverse polarizations of the gauge bosons have no thermal mass, so only longitudinal degrees of freedom receive a thermal mass contribution. This is directly derivable from the expression of the momentum-dependent gauge self-energy (Equation (2.24) is in the soft-limit, where it is independent of external momentum) [50]:

$$\Pi_T = m_{\text{GB, thermal}}^2 x [(1 - x^2)Q_0(x) + 1] \quad (2.25)$$

$$\Pi_L = \frac{m_{\text{GB, thermal}}^2 K^2}{k^2} (1 - xQ_0(x)) \quad (2.26)$$

where $Q_0(x)$ is the Legendre function of the second kind and $x \equiv \frac{k_0}{k}$. In the soft-limit $x \rightarrow 0$, so $\Pi_T = 0$ and $\Pi_L = m_{\text{GB, thermal}}^2$ as expected. Equations (2.22) and (2.24) can be checked for the values of the SM as calculated in [36]. As there are many different definitions used in papers for values as N_f or N_s , Equations (2.22) and (2.24) agree with the SM values, if one uses the following values. $N_f = 12 = (\text{spin})(\text{colour})(\text{particle/anti-particle})$ for the top-quark, $N_c = 3$, $N_s = 4$ as the complex Higgs doublet has four real degrees of freedom and $C_2(r_s) = \frac{3}{4}$ and $C_2(r_{GB}) = 2$ for the $SU(2)$ gauge bosons and $C_2(r_s) = \frac{1}{4}$ for $U(1)$. These thermal contributions to the SM particles are also given in Appendix A.

Now all the field theoretical tools are given and one can determine the effective potential of any model by combining Equations (2.2) and (2.13) with the tree-level potential from the Lagrangian and including the Daisy resummed thermal masses:

$$V_{\text{eff}}(\phi) = V^{(0)}(\phi) + V^{(1)}(\phi) + V_T^{(1)}(\phi, T) \quad (2.27)$$

However, there are constraints on what one could do. In the next chapter, numerous constraints are discussed, which will help with building conformal extensions of interest.

⁷Diagram (e) in Figure 2.5 is a ghost-loop diagram, which is gauge dependent. It is gauge fixed away in the final result, but for completeness the diagram is shown here.

⁸Note that this is not equal to the number of colours of the fermion N_c .

⁹Equations (2.22) and (2.24) have been checked by comparing them to multiple explicit values in literature [17, 36, 41, 49] and were correct apart from this factor of two, which was consistently incorrect. Before the finish of this thesis, the possible mistake in [42] was not found.

Chapter 3

Theoretical and experimental constraints

In the previous chapter, the field theoretical backgrounds need to build conformal extensions of the SM have been discussed. However, there do not seem to be any rules on what a conformal extension maker could put in these models. Could he or she just add any type of particle in any quantity and let it interact with other particles in whatever way the maker would want them to interact? The logical answer is no, there are multiple different aspects one needs to keep in mind when constructing a conformal model. In this chapter, several of these constraints from both experimental as theoretical fields of physics are discussed.

3.1 Relativistic degrees of freedom

One of the most important theoretical predictions by the most popular cosmological model, Λ CDM [51], is the existence of a relativistic energy component [52] at the time of the CMB. The radiation energy density of the Universe (besides the background of CMB photons) at decoupling is given by:

$$\rho_{\text{rad}} = \rho_{\gamma} \left(1 + \frac{7}{8} \left(\frac{4}{11} \right)^{\frac{4}{3}} N_{\text{eff}} \right) \quad (3.1)$$

where ρ_{γ} is the energy density of the CMB photons with a temperature of $T_{\gamma} = 2.728$ K today. The free parameter N_{eff} is the effective number of relativistic degrees of freedom. The SM predicts the value to be $N_{\text{eff}} = 3.046$ from the three neutrino flavours as neutrinos were still relativistic at the time of decoupling. The slight deviation from exactly three is due to neutrino flavour oscillations and some uncertainty from the fact that neutrinos likely did not decouple from the plasma instantaneously in the early Universe [53]. If one would introduce new particles, it should be checked if any are still relativistic (i.e. massless or very light) at time of decoupling. This would namely mean they would affect the expected value of N_{eff} .

The effective number of relativistic degrees of freedom can be experimentally found from observations of temperature and polarization anisotropies of the CMB. Current Planck data have found increasingly constrained values of $N_{\text{eff}} = 3.15 \pm 0.23$ for data up to 2015 [54] and even $N_{\text{eff}} = 2.99 \pm 0.17$ from data up to last year [53]. These values are consistent with the SM value and leave little to no room for any new particles contributing to N_{eff} .

3.2 CP-violation and baryogenesis

One of the bigger questions of cosmology is the asymmetry between baryonic matter and anti-matter with $\eta = (\eta_B - \eta_{\bar{B}})/\eta_{\gamma} = 6.176 \pm 0.148 \cdot 10^{-10}$ [55]. It is not possible that the

Universe started with a net number of baryons, as inflation predicts that this would be completely wiped out after a period of inflation. So apparently there has been a period in the early Universe¹, which allowed for baryogenesis, the net production of baryons. It was found by Sakharov that baryogenesis can occur in an Universe with baryon number equal to zero if three conditions hold [57]:

1. There must be reactions that change baryon number B
2. Charge (C) and charge-parity (CP) violation
3. Departure from thermal equilibrium

Violation of baryon number is obviously needed to produce more matter than anti-matter. However, C-symmetry would balance this with processes which produce more anti-matter than matter. Likewise, CP-symmetry would produce equal numbers of left-handed baryons as right-handed anti-baryons (and vice-versa). Lastly, thermal equilibrium has CPT-symmetry, which also could reverse any effects from CP violation. So one needs to be away from thermal equilibrium to break CPT-symmetry.

Even though the SM is able to fulfill all conditions, the asymmetry it can theoretically produce is too small to explain the existing amount of baryonic matter [58, 59]. The first condition can be fulfilled during an electroweak phase transition, however the Higgs mass is too small to induce a strong enough first-order transition in the SM. Furthermore, the amount of CP-violation is also not enough. This means that beyond the SM physics is needed to account for the measured asymmetry. And as will be seen in Chapter 5, conformal extensions of the SM naturally possess strong first-order electroweak phase transitions.

An straightforward example of how CP-violation can occur, can be seen from the following Yukawa interaction [60]:

$$-\mathcal{L}_{Yukawa} = Y_{ij}\bar{\psi}_{Li}\phi\psi_{Rj} + Y_{ij}^*\bar{\psi}_{Rj}\phi^\dagger\psi_{Li}$$

A CP-transformation would look this:

$$CP(\bar{\psi}_{Li}\phi\psi_{Rj}) = \bar{\psi}_{Rj}\phi^\dagger\psi_{Li}$$

This means that \mathcal{L}_{Yukawa} is CP-invariant if $Y_{ij} = Y_{ij}^*$. So in this case one can introduce "spontaneous CP-violation" by assuming a complex phase in Y_{ij} . This process, for example, is also the reason of the small CP-violation in the CKM matrix in the SM [61] and can also be introduced in new conformal extensions.

3.3 Vacuum stability

Any new scalar potential that is introduced for new physics beyond the Standard Model (BSM), must be bounded from below or in other words, vacuum stability is necessary up to the Planck scale. If the potential would not be bounded from below, a scalar affected by this potential could never find a lowest stable energy state. For a single scalar (e.g. the Standard Model Higgs boson) one can easily deduce the bounds by themselves. A quartic coupling $\lambda\phi^4$ is not bounded from below for $\lambda < 0$. However, for multiple scalars interacting with each other in a quadratic form $\lambda_{ab}\phi_a^2\phi_b^2$, this is not always obvious. In this thesis, only conformal models are considered, so there are only quartic terms in the scalar potential, but terms with dimensionful couplings could have been ignored anyway, since these terms are negligible compared to the quartic terms in the limit of large field values [62].

¹It can be shown that the asymmetry must have existed already at early times ($T \gtrsim 40\text{MeV}$), see e.g. [56] for a discussion.

As it turns out, the question of boundedness from below can be reduced to demanding that the matrix λ_{ab} is copositive² [62, 63]. For 2×2 - and 3×3 -matrices, the criteria for copositivity can be explicitly found. The following matrices are of interest for the models that will be introduced in Chapter 4.

:

$$A_{2 \times 2} = \frac{1}{8} \begin{pmatrix} 2\lambda_1 & \lambda_2 \\ \lambda_2 & 2\lambda_3 \end{pmatrix}$$

$$A_{3 \times 3} = \frac{1}{8} \begin{pmatrix} 2\lambda_1 & \lambda_2 & 0 \\ \lambda_2 & 2\lambda_3 & \lambda_4 \\ 0 & \lambda_4 & 2\lambda_5 \end{pmatrix}$$

The conditions for copositivity for $A_{2 \times 2}$ are:

$$\begin{aligned} \lambda_1 &\geq 0, \lambda_3 \geq 0 \\ \lambda_2 &\geq -2\sqrt{\lambda_1\lambda_3} \end{aligned} \quad (3.2)$$

and for the three-dimensional case $A_{3 \times 3}$:

$$\begin{aligned} \lambda_1 &\geq 0, \lambda_3 \geq 0, \lambda_5 \geq 0 \\ \lambda_2 &\geq -2\sqrt{\lambda_1\lambda_3} \\ \sqrt{\lambda_1\lambda_5} &\geq 0 \\ \lambda_4 &\geq -2\sqrt{\lambda_3\lambda_5} \end{aligned} \quad (3.3)$$

$$2\sqrt{\lambda_1\lambda_3\lambda_5} + \lambda_2\sqrt{\lambda_5} + \lambda_4\sqrt{\lambda_1} + \sqrt{(\lambda_2 + 4\sqrt{\lambda_1\lambda_3})(2\sqrt{\lambda_1\lambda_5})(\lambda_4 + 2\sqrt{\lambda_3\lambda_5})} \geq 0$$

The last statement is a simplification of either of the following two inequalities being true:

$$\begin{aligned} 2\sqrt{\lambda_1\lambda_3\lambda_5} + \lambda_2\sqrt{\lambda_5} + \lambda_4\sqrt{\lambda_1} &\geq 0 \\ \det A_{3 \times 3} = 8\lambda_1\lambda_3\lambda_5 - (\lambda_2^2\lambda_5 + \lambda_4^2\lambda_1) &\geq 0 \end{aligned} \quad (3.4)$$

The conditions in Equations (3.2) and (3.3) will be used in Chapter 6 to determine appropriate values for the coupling constants for the models that will be introduced in Chapter 4. As a taster, the $SU(2)$ -case for one of the models (the adjoint fSU(N)cSM in Section 4.3) is already given, as this is slightly different than the $A_{3 \times 3}$, which is applicable to the MfSU(N)cSM that is introduced in Section 4.4. The scalar potential for the adjoint fSU(N)cSM looks in matrix-form as:

$$A_{3 \times 3} = \frac{1}{8} \begin{pmatrix} 2\lambda_1 & \lambda_2 & \lambda_2 \\ \lambda_2 & 2\lambda_3 + 2\lambda_4 & 2\lambda_3 \\ \lambda_2 & 2\lambda_3 & 2\lambda_3 + 2\lambda_4 \end{pmatrix} \quad (3.5)$$

This gives the following copositivity constraints:

$$\begin{aligned} \lambda_1 &\geq 0, \quad \lambda_3 + \lambda_4 \geq 0 \\ \lambda_2 &\geq -2\sqrt{\lambda_1(\lambda_3 + \lambda_4)} \\ \lambda_3 &\geq -|\lambda_3 + \lambda_4| \\ 2|\lambda_3 + \lambda_4|\sqrt{\lambda_1} + 2\lambda_2\sqrt{\lambda_3 + \lambda_4} + 2\lambda_3\sqrt{\lambda_1} \\ &+ |(\lambda_2 + 2\sqrt{\lambda_1(\lambda_3 + \lambda_4)})\sqrt{2\lambda_3 + 2|\lambda_3 + \lambda_4|}| \geq 0 \end{aligned} \quad (3.6)$$

²Copositive is short for conditionally positive and a copositive matrix A is defined by $x^T Ax \geq 0$ for any non-negative vector $x \geq 0$. [62]

3.4 Dark matter relic abundance

In Section 4.1.4 it will be outlined how the newly added particles in conformal extensions can behave as possible dark matter candidates. There are some constraints on what cosmologists think dark matter should be. The most well known is the dark matter abundance in the Universe compared to the universal critical density ρ_c [53]:

$$\Omega_{\text{DM}} = \frac{\rho_{\text{DM}}}{\rho_c} = (0.12010 \pm 0.0012)h^{-2} \quad (3.7)$$

where $h \approx .7$ is the Hubble expansion rate today in units of 100 km per sec per Mpc. The relic dark matter abundance ρ_{DM} of a dark matter candidate is calculated from its number density n_{DM} time-dependence in thermal equilibrium and should not be higher than the experimentally found value [16]:

$$\frac{dn_{\text{DM}}}{dt} = -3Hn_{\text{DM}}(t) - (n_{\text{DM}}^2(t) - n_{\text{DM}}^{(eq)2})\langle\sigma v\rangle_{\text{annihilation}} \quad (3.8)$$

where the last term is the thermally averaged annihilation cross section of the dark matter candidate, which can be deduced from its interaction processes (see e.g. [64, 65]). A small sidenote, is that the annihilation process can inject energy into the intergalactic medium, which can be seen in the CMB. The parameter which can be constrained by CMB measurements is [53]:

$$p_{\text{ann}} \sim \frac{\langle\sigma v\rangle_{\text{annihilation}}}{m_{\text{DM}}} < 3.5 \cdot 10^{28} \text{ cm}^3 \text{ s}^{-1} \text{ GeV}^{-1} \quad (3.9)$$

3.5 Higgs boson mass and VEV

The current mass of the Higgs boson is $m_H = 125.09 \pm 0.21$ (stat.) ± 0.11 (syst.) GeV and the VEV is given by $\langle h \rangle = \frac{1}{\sqrt{\sqrt{2}G_F^0}} \approx 246.22$ GeV, where G_F^0 is the reduced Fermi constant [2]. Any proposed model will need to return these two values as they determine all the other (experimentally verified) masses of the SM. So these values will constrain the set of free parameters of new models.

3.6 LHC limits on heavy dark Higgs mass

The SM Higgs boson can decay into different other SM particles, but it can perhaps also decay into any new particles in a conformal extension. The exact decay width Γ is being more and more precisely measured, meaning the portal coupling to a dark sector such as in the discussed models in this thesis, becomes more and more constrained. One can write down the decay rate for a scalar particle h in these models:

$$\Gamma_h^{\text{tot}} = \eta \Gamma_h^{\text{SM}} + \Gamma_h^{\text{dark}} \quad (3.10)$$

Here η is a measure of how much of the total decay width is determined by the 'visible' decays in the SM. The decay width is not directly measurable, but ATLAS and CMS have been able to constrain the signal strength parameter $\mu_h > 0.81$ [3, 4], defined by:

$$\begin{aligned} \mu_h &= \frac{\sigma(pp \rightarrow h)}{\sigma^{\text{SM}}(pp \rightarrow h_{\text{SM}})} \frac{BR(h \rightarrow \chi\chi)}{BR^{\text{SM}}(h_{\text{SM}} \rightarrow \chi\chi)} \\ &= \eta^2 \frac{\Gamma_h^{\text{SM}}}{\Gamma_h^{\text{tot}}} \\ &\approx \eta \end{aligned} \quad (3.11)$$

Here σ and BR are the production cross section and branching ratios of the candidate Higgs particle h in our models and the SM Higgs h_{SM} . The particles χ are all the SM-particles into which the Higgs boson can decay (i.e. quarks, leptons and gauge bosons).

In the last step, it is used that $\Gamma_h^{\text{dark}} \ll \eta \Gamma_h^{\text{SM}}$ along with Equation (3.10). So this results in the constraint $\eta > 0.81$, where η can be calculated from the interaction terms in the Lagrangian of the different models. To circumvent the problem discussed here, the general assumption is that the Higgs-like scalar in these models is the lightest of the scalars, so decay to dark scalars is kinetically not allowed. Likewise, only dark particles with $M_{\text{dark}} \lesssim 62.5$ GeV can be the products of the Higgs boson decay.

It is not the aim of this thesis to rigorously check for the models if the theoretical decay width will exceed the experimental bounds, yet it is of importance to note that future upgrades of the LHC will be able to severely constrain any possible conformal extensions. It is always possible to choose the free parameters in such a way that the massive particles in the dark sector are heavy enough. It could be that not all particles attain a mass for certain symmetry breaking patterns (see also Section 4.1.4), which could complicate satisfying the constraint. However, this would also be problematic for the effective number of relativistic degrees of freedom, as discussed in Section 3.1.

3.7 Perturbativity

Closely related to the constraint of vacuum stability of the model up to the Planck scale is the requirement that the model must also be perturbative up to the Planck scale $\sim M_P \approx 2.435 \cdot 10^{18}$. This is achieved by requiring all running coupling constants to be bounded by 2π [14]. For a specific model, this is determined by considering all the renormalization group equations and solve them. Typically as boundary conditions for these differential equations the values at the energy scale of the top quark mass $M_t \sim 173$ GeV are used. For general gauge groups, all two-loop renormalization group equations can be found in [66].

In this chapter, a list of theoretical and experimental constraints on conformal extensions of the SM have been given. Not all are directly as relevant for this thesis, as the aim is to see what types of conformal extensions can be made. Therefore the constraints used in this thesis are the ones mentioned in Sections 3.2, 3.3 and 3.5. The other constraints are left for future research. Now one can turn to actually introducing new conformal extensions of the SM in the next chapter.

Chapter 4

Examples of conformal extensions

In constructing a dark matter model, there is a wild variety of choices one can make and only a limited number of limitations (see Chapter 3) . One could say that "anything goes". However, by demanding a conformal model with (potentially) experimentally measurable signatures, there are some statements one can make. To begin with, one would like a phase transition to be possible in the scalar part of the theory to ensure a measurable signature. More specifically, the general aim is to construct a model in such a way that a strong first-order phase transition occurs, which in turn can be seen via gravitational waves. Analyzing the symmetry-breaking patterns of general models and thus finding phase transitions is done in Section 4.1.

In Chapter 2 the general field theory techniques needed to build a conformal extension to the SM have been discussed. As doing this for a specific model is not a trivial task, three examples are studied in this chapter. The first model is the $SU(2)$ cSM [15] and is perhaps the most minimal way of constructing a conformal model, as will be discussed in Section 4.2. As this model has been studied already, it is used in later chapters as a benchmark for numerical calculations. Then two new models will be introduced, which have a larger zoo of particles. This will come with extra difficulties during construction, but will also yield more interesting characteristics¹.

4.1 Symmetry-breaking in general gauge groups

Before one can identify the symmetry breaking in a specific model, there is need to explore which gauge groups are of interest and how they could reduce to lower rank symmetry groups. Because in this case, it is found that not everything is possible and gauge groups are even severely restricted in how they can break the symmetry.

This field has been heavily researched in the seventies, when an unification was found between electromagnetism and the weak interaction by Glashow, Salam and S. Weinberg [33–35]. The belief (or hope) was that the other forces could also be unified by a Grand Unified Theory (GUT) in a larger symmetry group. This intensified research into symmetry breaking from all kinds of symmetry groups, since there was little experimental data to rule out much.² One could say that the current field of dark matter is at a similar point in terms of experimental knowledge and thus freedom in choosing symmetry groups for dark matter models. Therefore one can luckily rely on the research done in the '70s.

Considering the Standard Model turned out to be a collection of unitary gauge groups

¹See 3.

²Notable exceptions from this are the absence of proton decay ruling out $SU(5)$ and constraints due to the absence of magnetic monopoles.

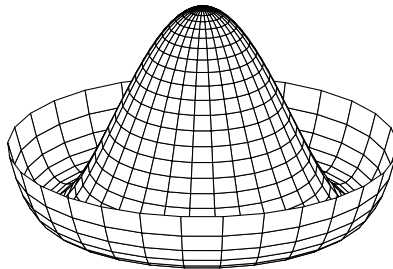


Figure 4.1: The mexican hat potential for a scalar particle with a $U(1)$ symmetry

($SU(3) \times SU(2) \times U(1)$), this discussion of possible symmetry breakings will restrict itself to the groups $SU(N)$ and the special orthogonal groups $SO(N)$ seeing that they behave rather similar.

4.1.1 Symmetry breaking patterns in $SU(N)$ and $SO(N)$

The question of how symmetry breaking takes place is in essence a geometrical problem of what symmetries are preserved if the global minimum is no longer at the origin. The easiest example is the well-known "Mexican hat"-potential for a $U(1)$ symmetric scalar particle as shown in Figure 4.1.

The particle has a $U(1)$ symmetry at its maximum, but can roll down the potential in any given direction and spontaneously break the symmetry. In the case of $SU(N)$ and $SO(N)$, the problem is similar, but multidimensional and therefore impossible to visually solve.

In a very mathematical approach to generally find the symmetry breaking pattern for a quartic Higgs potential, it was conjectured in 1971 [67] that any irreducible representation of a symmetry group G breaks down to its maximal little groups³ on its minima.

4.1.2 Example of a symmetry breaking analysis

This is explicitly proven for different representations of $SU(N)$ and $SO(N)$ in [68–71], but a more conventional (i.e. less technical) method was used by Li in [72] along with some corrections in [73]. To show how a symmetry breaking pattern can be found for a particular symmetry group, one can consider the example of the second-rank symmetric tensor in the $O(N)$ group, which is completely analog to the adjoint representation of $SU(N)$ [72].

In this case, the scalar field has the symmetric property $\phi_{ij} = \phi_{ji}$ and also $\text{Tr}\{\phi\} = 0$. The most general potential, including the assumption that a mass term μ for the scalar is generated via an unspecified mechanism, can be written as:

$$V(\phi) = -\frac{1}{2}\mu^2(\phi_{ij}\phi_{ji}) + \frac{1}{4}\lambda_1(\phi_{ij}\phi_{ji})^2 + \frac{1}{4}\lambda_2(\phi_{ij}\phi_{jk}\phi_{kl}\phi_{li}) \quad (4.1)$$

$$\text{or equivalently:} \quad = -\frac{1}{2}\mu^2 \text{Tr}[\phi^2] + \frac{1}{4}\lambda_1 \text{Tr}[\phi^2]^2 + \frac{1}{4}\lambda_2 \text{Tr}[\phi^4] \quad (4.2)$$

where now the analog to the $SU(N)$ adjoint representation is obvious. As the matrix ϕ is real and symmetric, it can be diagonalized: $\phi_{ij} = \delta_{ij}\phi_i$ with $i = 1, \dots, N$. However, the components ϕ_i are not all independent, because of the trace condition. By adding a Lagrange multiplier g to the potential, this is taken into account:

$$V(\phi) = -\frac{1}{2}\mu^2 \sum_i \phi_i^2 + \frac{1}{4}\lambda_1 \left(\sum_i \phi_i^2 \right)^2 + \frac{1}{4}\lambda_2 \sum_i \phi_i^4 - g \sum_i \phi_i \quad (4.3)$$

³The definition of a maximal little is group is the largest group, which does not contain an other maximal little group, that contains singlets in its subrepresentations.

Then the minimum of this potential is given with the following condition:

$$\frac{\partial V}{\partial \phi_i} = \mu^2 \phi_i + \lambda_1 \phi_i \sum_j \phi_j^2 + \lambda_2 \phi_i^3 - g = 0 \quad (4.4)$$

Interestingly, one can prove that ϕ_i can only take three different values ϕ_1, ϕ_2 and ϕ_3 . They each must satisfy Equation (4.4). By subtracting one from the others, the conditions become:

$$-\mu^2 + \lambda_1 \sum_j \phi_j^2 + \lambda_2(\phi_1^2 + \phi_1\phi_2 + \phi_2^2) = 0 \quad (4.5)$$

$$-\mu^2 + \lambda_1 \sum_j \phi_j^2 + \lambda_2(\phi_1^2 + \phi_1\phi_3 + \phi_3^2) = 0 \quad (4.6)$$

One can again subtract these equations from each other, yielding the simple condition:

$$\phi_1 + \phi_2 + \phi_3 = 0 \quad (4.7)$$

If there would have been another distinct solution ϕ_4 , the same procedure could be done to find $\phi_2 + \phi_3 + \phi_4 = 0$. However, this must imply that $\phi_1 = \phi_4$, so indeed only three different values for ϕ_i are possible. So ϕ can be written as a diagonal matrix with n_1 entries of ϕ_1 , n_2 entries for ϕ_2 and n_3 entries for ϕ_3 :

$$\phi_1 + \phi_2 + \phi_3 = 0 \quad (4.8)$$

$$n_1 + n_2 + n_3 = N \quad (4.9)$$

$$n_1\phi_1 + n_2\phi_2 + n_3\phi_3 = 0 \quad (4.10)$$

The last condition is just the trace condition and the set of equations means that ϕ_2 and ϕ_3 can be written in terms of ϕ_1 and the potential can be written as:⁴

$$V(\phi) = -a(n_1, n_2, n_3)\phi_1^2 + b(n_1, n_2, n_3)\phi_1^4 \quad (4.11)$$

Now minimizing the potential with respect to ϕ_1 and one yields the potential value at the minimum:

$$V_m = -\frac{\mu^4}{4} \frac{1}{\lambda_1 + \lambda_2 f(n_1, n_2, n_3)} \quad (4.12)$$

From this, one can now deduce the smallest minimum by determining the values for n_1 , n_2 and n_3 , which yield the minimum or maximum value of f . This depends on if λ_1 and λ_2 are negative or positive. In summary, one can find that the possible symmetry breaking patterns are:

- $O(N) \rightarrow O(\lceil \frac{N}{2} \rceil) \times O(\lfloor \frac{N}{2} \rfloor)$ for $\lambda_1 > 0$ and $\lambda_2 > 0$
- $O(N) \rightarrow O(N-1)$ for $\lambda_1 > 0$ and $\lambda_2 < 0$

So this example shows how one can systematically determine possible symmetry breaking patterns in the presence of a mass term for a certain symmetry group and representation of ϕ .

⁴The exact expressions of a and b , as well as f are not given here, as they are too lengthy and not needed for the purpose of this section. They can be found in Appendix C.

4.1.3 Resulting symmetry breaking patterns

Now a general overview of the possible resulting symmetry breaking patterns are given below for scalar particles in the fundamental and adjoint representations. Li also discusses (anti-)symmetric tensors, but for the simplicity of this thesis, these are not considered here.

- Single dark scalar in the fundamental representation

$$SU(N) \implies SU(N-1)$$

$$SO(N) \implies SO(N-1)$$
- k dark scalars in the fundamental representation

$$SU(N) \implies SU(N-k)$$

$$SO(N) \implies SO(N-k)$$
- Single dark scalar in the adjoint representation

$$SU(N) \implies SU(\lceil \frac{N}{2} \rceil) \times SU(\lfloor \frac{N}{2} \rfloor) \times U(1)$$

$$SO(N) \implies SO(N-2)$$

The adjoint result for $SO(N)$ is taken from [69]. Note that in the case of multiple scalars for $SU(N)$ and $SO(N)$, it is possible to break the symmetry completely by adding $k = N - 1$ scalars. The given patterns are for a negative coupling constant, which is required from the boundedness from below of the potential, which will be explained in detail later in 3.3.

Another possibility is to let the scalar particle transform under two representations⁵, which has also been studied by, among others, Li. However, again for the sake of simplicity, these options are ignored. One can note that it is not always the case that the symmetry completely breaks down, but that there will be a leftover symmetry group. For now, it can be concluded that typically $SU(N)$ and $SO(N)$ gauge groups have very clear symmetry breaking patterns. This can be used to predict the behaviour of conformal extensions as the relic symmetries will also behave in a certain way in nature. In the next section it will be made clear what these remaining symmetry groups can be.

4.1.4 Resulting particle behaviour of symmetry groups

As the previous section has shown, symmetry breaking can leave a residual symmetry in the hidden sector. These symmetries determine the present day behaviour of the particles in the extension. These particles could be very natural candidates for dark matter as they are weakly-interacting with the SM particles. So it is of interest to consider different types of relic symmetries and how they could behave as possible dark matter candidates.

$SU(m)$ symmetry

The most interesting relic symmetry would be the non-Abelian gauge group $SU(m)$. The gauge bosons in such a group are the dark analogue of QCD and they can self-interact for even the simplest possible extensions [74] without any additional matter content. It is theorized that QCD has bound states of gluons, called glueballs, as gluons can self-interact. There has not been any experimental evidence for this, but the theoretical evidence is strong [75]. Likewise, the self-interaction of a non-abelian gauge group in the hidden sector could also theoretically produce bound states. As in literature, these gauge bosons are mostly referred to as X-bosons, these bound states could be referred to as 'X-balls'. If these X-balls have a lifetime of the order of the age of the Universe or larger, they can account for the observed dark matter relic density. This mainly depends on the temperature scale Λ at which the X-bosons go from a plasma to the confined state of X-balls and the number of degrees of freedom $g_{\text{eff}} = 2(m^2 - 1)$. Experimentally, Λ is constrained by the self-interaction cross section and lies rather close to $\Lambda_{QCD} \sim 300\text{MeV}$ [74]. In conclusion, depending on the exact particle spectrum in the hidden sector apart from the $SU(m)$ gauge group, the gauge bosons could be a viable dark matter candidate.

⁵In representation form, that would be for example (\mathbf{M}, \mathbf{N}) for the two groups $SU(N)$ and $SU(M)$.

$U(1)$ symmetry

A relic $U(1)$ symmetry needs a Z_2 symmetry to give stable particles, which corresponds to a charge conjugation symmetry [76]. Through symmetry breaking the gauge field must have become massive and is the natural DM candidate [65]. If the gauge field is massless, one has 'dark electromagnetism' with a corresponding dark photon [77]. However, relativistic degrees of freedom are heavily constrained by Planck (see Section 3.1 for the complete discussion) and thus are dark photons likely not a viable option.

Another interesting option for dark matter is the possibility of cosmic strings, which can be created by local $U(1)$ symmetry [78]. However, this is outside the scope of this thesis.

4.2 The benchmark model: SU(2)cSM

As have been argued, extending the SM with one singlet scalar field would require a large coupling between the Higgs doublet and the singlet. However, this also leads to a Landau pole below the Planck scale ($\sim 10^{16}$ GeV) [10]. The simplest way to overcome this, is by gauging the new scalar field under a new gauge group, while keeping it singlet under the SM gauge groups. So one could state that the most minimal classically conformal with an extended scalar (and gauge) sector is by considering a new scalar Φ acting as a doublet under a new gauge group $SU(2)_X$.⁶ This whole sector acts trivially under the SM gauge groups to ensure that experimental measurements of the SM are not affected. The model is referred to as the SU(2)cSM [10, 15, 64, 81]. The scalar potential for SU(2)cSM is given by:

$$V^{(0)}(H, \Phi) = \lambda_1(H^\dagger H)^2 + \lambda_2(H^\dagger H)(\Phi^\dagger \Phi) + \lambda_3(\Phi^\dagger \Phi)^2 \quad (4.13)$$

Here H is the SM scalar doublet and there are four free parameters λ_1 (the 'old' self-coupling of the SM Higgs), λ_2 , λ_3 and g_X , where g_X is the gauge coupling constant of the $SU(2)_X$ gauge group. It has been found that RSB can take place in SU(2)cSM and can reproduce the correct particle spectrum of the SM for a wide range of different parameter choices [10]. Two of the parameters are fixed by the known experimental values of the Higgs boson mass and VEV, which has been explained in Section 3.5.

4.2.1 Mass eigenvalues of SU(2)cSM

Of experimental interest for the phenomenology of this model at the present day are the zero temperature mass eigenvalues, which follow from the zeroth order effective potential:

$$V^{(0)}(h, \phi) = \frac{1}{4}(\lambda_1 h^4 + \lambda_2 h^2 \phi^2 + \lambda_3 \phi^4) \quad (4.14)$$

Here the two symmetries of the potential, the weak $SU(2)$ and $SU(2)_X$, are used to rewrite the classical tree-level potential in terms of only the radial fields h and ϕ . The two corresponding background fields in the effective potential will be denoted by $\vec{h} = (0, 0, 0, h)$ and $\vec{\phi} = (0, 0, 0, \phi)$ as well to illustrate their origin.

Now one can compute the scalar masses by simply calculating the Hessian of the tree-level potential:

⁶ $SU(2)$ is the simplest gauge group one can consider, as the coupling constant in the smaller gauge group $U(1)$ generically develops a Landau pole. There do exist exceptions for certain choices of parameters (see e.g. [79, 80]).

$$m_{h,\phi}^2(h,\phi) = \frac{1}{2} \left(3\lambda_1 + \frac{\lambda_2}{2} \right) h^2 + \frac{1}{2} \left(3\lambda_3 + \frac{\lambda_2}{2} \right) \phi^2 \pm \sqrt{\left[\left(3\lambda_1 + \frac{\lambda_2}{2} \right) h^2 - \left(3\lambda_3 + \frac{\lambda_2}{2} \right) \phi^2 \right]^2 + 4\lambda_2^2 h^2 \phi^2} \quad (4.15)$$

$$m_{G,G^\pm}^2(h,\phi) = \lambda_1 h^2 + \frac{\lambda_2}{2} \phi^2 \quad (4.16)$$

$$m_{\tilde{G},\tilde{G}^\pm}^2(h,\phi) = \lambda_3 \phi^2 + \frac{\lambda_2}{2} h^2 \quad (4.17)$$

Here $G^{(\pm)}$ and $\tilde{G}^{(\pm)}$ are the Goldstone bosons of the weak and $SU(2)_X$ sector, respectively. The gauge bosons in the new sector are referred to as X-bosons and thus the other massive particles are given by:

$$\begin{aligned} m_W(h) &= \frac{gh}{2} & , & \quad m_Z(h) = \frac{\sqrt{g^2 + g'^2}h}{2} \\ m_X(\phi) &= \frac{g_X\phi}{2} & , & \quad m_t(h) = \frac{y_t h}{\sqrt{2}} \end{aligned} \quad (4.18)$$

In further calculations the Goldstone contributions are neglected. They have been shown to be negligible [10] and furthermore carry all the gauge dependence, leaving the effective potential approximately gauge independent if they are left out. Also, only the top quark is considered as the masses of the other quarks are so small that they do not effect the calculations enough to be of importance. Both these choices will also be made in the models that will be introduced in the next sections.

One can now write down the full effective potential using Equations (2.2) and (2.13) and the thermal mass corrections are given in Appendix A. As has been explained, only the scalars and the longitudinal gauge bosons gain thermal masses. The study of the phase transition of $SU(2)$ cSM will be done in Chapter 5.

As was discussed in Chapter 3, there are many characteristics conformal extensions can have that are relevant in different fields of research. Most notably, these types of models can contain dark matter candidates or have CP-violating interactions, which could explain matter-anti-matter inequality. That is why it is interesting to consider not just the most minimal model, but also more complicated gauge groups and possibly extra fermionic degrees of freedom. So that is why two new models are introduced in the next two sections.

4.3 The adjoint fSU(N)cSM

Part of the original goal of this thesis was to analyze the dependence of signatures of the model (i.e. gravitational wave spectra as will be shown in Chapter 6) on the models new gauge group. Therefore it is of interest to construct a model with a general gauge group in its new sector, which has degree N . If the degree is kept general, little change is expected compared to the $N = 2$ case, which is $SU(2)$ cSM, as it is still possible to write down the potential in terms of radial fields and the other Goldstone fields are neglected. The only difference is then the number of gauge bosons. This means that the phase transition will evolve in a similar way, but the strength of the transition will slightly increase [18]. However, one could also choose the new scalar to be in a different representation than the fundamental representation.

An obvious choice would be the adjoint representation, which has not been studied

extensively yet.⁷ The last ingredient for this model will be a set of Dirac fermions, also gauged under the SU(N)-symmetry and a Yukawa coupling with the scalar fields and coupling strength y_X . These fermions will get their mass via the adjoint scalar and can possibly induce CP-violating interactions.

So to summarize, the model contains a SU(N) gauge group with $N^2 - 1$ gauge bosons X, a scalar in the adjoint representation of this gauge group and N gauged Dirac fermions. As any model needs a proper name, this model will be referred to as the adjoint fSU(N)cSM in the remainder of this thesis, where f stands for the added fermions. This means one can write down the following tree-level potential (with at least two scalar field terms):

$$V^{(0)} = \lambda_1 (H^\dagger H)^2 + \lambda_2 (H^\dagger H) \text{Tr} [\Phi^2] + \lambda_3 \text{Tr} [\Phi^2]^2 + \lambda_4 \text{Tr} [\Phi^4] \quad (4.19)$$

The full Lagrangian is given in Appendix A. So for this model a set of six new parameters is introduced: ($\lambda_1, \lambda_2, \lambda_3, \lambda_4, g_X$ and y_X) and there is a general dependence on N . Again two of these parameters are fixed through the experimental Higgs mass and VEV.

Just as for the SU(2)cSM model, global symmetries can be used to simplify the expressions. However, this is different for the adjoint representation. A scalar field in the adjoint representation is a hermitian and symmetric $N \times N$ -matrix with complex fields ϕ_i^j and the trace identity $\phi_i^i = 0$, which indeed yields $N^2 - 1$ degrees of freedom as expected. Hermitian, symmetric matrices are always diagonalizable [72], so the matrix can be rewritten in terms of N real scalar fields ϕ_i (as the matrix must still be Hermitian). This means the potential can be rewritten with the following sets of reparametrizations:

$$\begin{aligned} 2 (H^\dagger H) &= \sum_{i=1}^4 h_i^2 \equiv h^2 \quad , \quad 2 \text{Tr} [\Phi^2] = \sum_{i=1}^N \phi_i^2 \equiv \phi^2 \\ 4 \text{Tr} [\Phi^4] &= \sum_{i=1}^N \phi_i^4 \end{aligned} \quad (4.20)$$

It is not possible to rewrite $\sum \phi_i^4$ into only terms depending on ϕ^2 ,⁸ thus in this model $N + 1$ fields must be considered instead of the two fields in SU(2)cSM. This will make it harder to analyze any characteristics of this model. So in terms of real scalar fields h and ϕ_i , the tree-level potential becomes:

$$V^{(0)}(h, \phi_i) = \frac{\lambda_1}{4} h^4 + \frac{\lambda_2}{4} h^2 \left(\sum_{i=1}^N \phi_i^2 \right) + \frac{\lambda_3}{4} \left(\sum_{i=1}^N \phi_i^2 \right)^2 + \frac{\lambda_4}{4} \sum_{i=1}^N \phi_i^4 \quad (4.21)$$

4.3.1 Mass eigenvalues

The next step is to determine the mass eigenvalues from the Hessian of the tree-level potential in Equation (4.21). Remembering that $h^2 = \sum h_i^2$, the following second derivatives are computed:

⁷An example would be [16], however they do not include the second quartic trace term in the tree-level potential. That means they do not consider the most general possible model and it also greatly simplifies calculations of the mass eigenvalues, as will become apparent further down.

⁸In [70] a method is mentioned to do this by introducing a new parameter $\lambda' = \lambda_3 + \alpha\lambda_4$. However, α is a rescaling parameter of the scalar fields and thus make λ' field-dependent: $\lambda'(\phi)$. Argumentation for the validity of this rescaling can be found in [68], but it is unclear how this would affect the behaviour of the model. It could be of interest in future research to compare this method with the general model.

$$\frac{\partial^2 V^{(0)}}{\partial h_a \partial h_b} = \delta_{ab} \left(\lambda_1 h^2 + \frac{\lambda_2}{2} \sum_{i=1}^N \phi_i^2 + 2\delta_{a4} \lambda_1 h^2 \right) \quad (4.22)$$

$$\frac{\partial^2 V^{(0)}}{\partial \phi_a \partial \phi_b} = \delta_{ab} \left(\frac{\lambda_2}{2} h^2 + \lambda_3 \sum_{i=1}^N \phi_i^2 + 3\lambda_4 \phi_a^2 \right) + 2\lambda_3 \phi_a \phi_b \quad (4.23)$$

$$\frac{\partial^2 V^{(0)}}{\partial h_a \partial \phi_b} = \delta_{a4} \lambda_2 h \phi_b \quad (4.24)$$

Here the indices a, b run from $1, \dots, 4$ for h_a and from $1, \dots, N$ for ϕ_a . It is clear that there will be mixing terms between the Higgs field and the new scalar fields from the last line in Equation (4.22). The masses of the SM Goldstone bosons are found to be:

$$m_{G, G^\pm}^2(h, \phi) = \lambda_1 h^2 + \frac{\lambda_2}{2} \phi^2 \quad (4.25)$$

which is similar to SU(2)cSM as found in Equation (4.15). The other masses are more difficult to compute, as it requires to find the eigenvalues of a $(N+1) \times (N+1)$ -matrix, which is not generically possible analytically. However, as this matrix is again Hermitian and symmetric and now all the entries are real, it must be possible to diagonalize the matrix. Which is the same as saying that there exist eigenvalues of this matrix and in this case the eigenvalues must also be real, even though no analytical expressions for the eigenvalues can be given.

So, unfortunately, it is not possible to give analytical expressions for the scalar particles in this model with a general dependence on N . To be able to study possible phase transitions within this model, two different scenarios are studied. First, the large- N limit is considered, comparable to the theory proposed by 't Hooft to construct a field theory for the strong interactions [82]. Secondly, the explicit case of $N = 2$ is considered.

The masses for the SM-particles remain unchanged and can be found in Appendix A. The masses of the X-bosons are given by $m_X^2 = \frac{g_X^2}{4} (\phi_1^2 + \phi_2^2)$ and the masses of the, in this case two, fermions are $m_{\psi_{1,2}}^2 = \frac{y_X^2}{8} \phi_{1,2}^2$.

4.3.2 Eigenvalues in large- N limit

In the large- N limit one has to explicitly keep track of the N -dependence of all terms in the tree-level potential. By doing this properly, one can ultimately calculate the Hessian in orders of N and ignore any sub-leading terms. The explicit dependence on N is found most easily⁹ by rewriting the potential in its generator basis t^a with $a = 1, \dots, N^2 - 1$ for the adjoint representation of SU(N). For this, the following identities from SU(N) group theory are needed [83, 84]:

$$\Phi = \sum_a \phi_a t^a \quad (4.26)$$

$$\text{Tr}[t^a t^b] = N \delta_{ab} \quad (4.27)$$

$$\text{Tr}[t^a t^b t^c t^d] = \delta_{ad} \delta_{bc} + \frac{1}{2} (\delta_{ab} \delta_{cd} + \delta_{ac} \delta_{bd}) + \frac{N}{4} \sum_e (f_{ade} f_{bce} + d_{ade} d_{bce}) \quad (4.28)$$

$$\sum_e d_{ade} d_{bce} = \frac{1}{3} \sum_e (f_{abe} f_{dce} + f_{ace} f_{dbe}) + \delta_{ab} \delta_{dc} + \delta_{ac} \delta_{db} - \delta_{ad} \delta_{bc} \quad (4.29)$$

$$\sum_a \epsilon^{abc} \epsilon^{aef} = \delta_{be} \delta_{cf} - \delta_{bf} \delta_{ec} \quad (4.30)$$

⁹'t Hooft originally constructed new Feynmann rules and summed the new diagrams, but for this case that is not necessary.

These identities can be used to rewrite the terms in the potential:

$$\text{Tr}[\Phi^2] = \sum_{a,b} \phi_a \phi_b \text{Tr}[t^a t^b] = N \sum_{a,b} \phi_a \phi_b \delta_{ab} = N \sum_a (\phi_a)^2 \quad (4.31)$$

$$\text{Tr}[\Phi^2]^2 = N^2 \left(\sum_a (\phi_a)^2 \right)^2 \quad (4.32)$$

$$\begin{aligned} \text{Tr}[\Phi^4] &= \sum_{a,b,c,d} \phi_a \phi_b \phi_c \phi_d \text{Tr}[t^a t^b t^c t^d] \\ &= \sum_{a,b,c,d} \phi_a \phi_b \phi_c \phi_d \left[\delta_{ad} \delta_{bc} + \frac{1}{2} (\delta_{ab} \delta_{cd} + \delta_{ac} \delta_{bd}) + \frac{N}{4} \sum_e (f_{ade} f_{bce} + d_{ade} d_{bce}) \right] \\ &= 2 \sum_{a,b} (\phi_a)^2 (\phi_b)^2 + \frac{N}{4} \sum_{a,b,c,d,e} d_{ade} d_{bce} \\ &= 2 \sum_{a,b} (\phi_a)^2 (\phi_b)^2 + \frac{N}{12} \sum_{a,b,c,d} \left(\sum_e (f_{abe} f_{dce} + f_{ace} f_{dbe}) + \delta_{ab} \delta_{dc} + \delta_{ac} \delta_{db} - \delta_{ad} \delta_{bc} \right) \\ &= 2 \sum_{a,b} (\phi_a)^2 (\phi_b)^2 + \frac{N}{12} \sum_{a,b} (\phi_a)^2 (\phi_b)^2 \\ &= \frac{N-24}{12} \sum_{a,b} (\phi_a)^2 (\phi_b)^2 \end{aligned} \quad (4.33)$$

The final step is to compute the Hessian:

$$\begin{aligned} \frac{\partial^2 V^{(0)}}{\partial \phi_x \partial \phi_y} &= 4N^2 \lambda_3 (\delta_{xy} \sum_a (\phi_a)^2 + 2\phi_x \phi_y) \\ &\quad + N \left(\lambda_2 \delta_{xy} h^2 + \frac{\lambda_4}{3} (\delta_{xy} \sum_a (\phi_a)^2 + 2\phi_x \phi_y) \right) \\ &\quad - 8\lambda_4 \left(\delta_{xy} \sum_a (\phi_a)^2 + 2\phi_x \phi_y \right) \end{aligned} \quad (4.34)$$

$$\frac{\partial^2 V^{(0)}}{\partial h_x \partial \phi_y} = \delta_{x4} N \lambda_2 h \phi_y \quad (4.35)$$

The λ_3 -terms are leading order $\mathcal{O}(N^2)$, whereas λ_2 and λ_4 contributions to the Hessian are only of order $\mathcal{O}(N)$. So from this, one can conclude that to leading order in N the mass spectrum of Φ should only depend on λ_3 and the other terms are negligible. This yields the following set of scalar masses:

$$m_\phi^2(\phi) = 12N^2 \lambda_3 \phi^2 \quad (4.36)$$

$$m_G^2(\phi) = 4N^2 \lambda_3 \phi^2 \quad (4.37)$$

Here there are $N-1$ Goldstone bosons with mass m_G^2 . One can deduce from this that for large N , the adjoint representation behaves similar to the fundamental representation.

4.3.3 Eigenvalues for $N = 2$: the adjoint fSU(2)cSM

The matrix that needs to be diagonalized is $(N+1)$ -dimensional. This is the same as trying to solve a polynomial of degree $N+1$, which is only possible for $N=2,3$. As the analytical solution for a polynomial of degree 4 becomes incredibly unwieldy, in this thesis only the case of $N=2$ (i.e. a polynomial of degree 3) is considered.

For $N = 2$, there are two new scalar fields ϕ_1 and ϕ_2 . according to Equation (4.22) the following matrix must be diagonalized:

$$M = \begin{pmatrix} A & B & C \\ B & D & E \\ C & E & F \end{pmatrix} \quad (4.38)$$

where

$$A = 3\lambda_1 h^2 + \lambda_2(\phi_1^2 + \phi_2^2)$$

$$B = \lambda_2 h \phi_1$$

$$C = \lambda_2 h \phi_2$$

$$D = \frac{\lambda_2}{2} h^2 + 3(\lambda_3 + \lambda_4)\phi_1^2 + \lambda_3\phi_2^2$$

$$E = 2\lambda_3\phi_1\phi_2$$

$$F = \frac{\lambda_2}{2} h^2 + 3(\lambda_3 + \lambda_4)\phi_2^2 + \lambda_3\phi_1^2$$

Now one can write down the characteristic polynomial in terms of quantities of the matrix M using basic linear algebra:

$$\alpha \equiv \text{Tr}[M] = A + D + F \quad (4.39)$$

$$\beta \equiv \det[M] = ADF - C^2D - E^2A - B^2F + 2BCE \quad (4.40)$$

$$\gamma \equiv \text{Tr}[M^2] = A^2 + D^2 + F^2 + 2(B^2 + C^2 + E^2) \quad (4.41)$$

$$0 = l^3 - \alpha l^2 + \frac{1}{2}(\alpha^2 - \gamma)l - \beta \quad (4.42)$$

The last line is the characteristic polynomial one has to solve to find the eigenvalues l . The solution is exactly known and given by:

$$l_k = -\frac{1}{3} \left(-\alpha + \xi^{k-1}\Xi + \frac{\alpha^2 - \frac{3}{2}(\alpha - \gamma)}{\xi^{k-1}\Xi} \right) \quad \text{for } k \in \{1, 2, 3\} \quad (4.43)$$

where

$$\xi = -\frac{1}{2} + \frac{1}{2}\sqrt{3}i \quad (\text{cubic root of } 1)$$

$$\Xi = \sqrt[3]{-\alpha^3 + \frac{9}{4}\alpha(\alpha - \gamma) - \frac{27}{2}\beta + \frac{1}{2}\sqrt{-27\Delta}} \quad \text{and}$$

$$\Delta = \frac{1}{4} (-\alpha^6 + 20\alpha^3\beta - 108\beta^2 + 4\alpha^4\gamma - 36\alpha\beta\gamma - 5\alpha^2\gamma^2 + 2\gamma^3)$$

Even though it was already determined for the general matrix that the eigenvalues should be real, this is not immediately obvious from this expression. This is due to the so called rule of *casus irreducibilis* [85], which states that the expression can be real despite the fact that it cannot be written without complex numbers. However, this is not the only problem with Equation (4.43). As it turned out, the expression is not well handled by the numerical program CosmoTransitions, which will be introduced in Chapter 6. This is solved by using an alternative geometrical expression from [86], which is better suited for numerical computations. It dictates an algorithm, which yields the following eigenvalues:

$$l_1 = \frac{\alpha}{3} + \sqrt{\frac{6\gamma - 2\alpha}{9}} \cos(\delta) \quad (4.44)$$

$$l_2 = \frac{\alpha}{3} - \sqrt{\frac{6\gamma - 2\alpha}{9}} \left(\frac{1}{2} \cos(\delta) - \frac{1}{2} \sqrt{3} \sin(\delta) \right) \quad (4.45)$$

$$l_3 = \frac{\alpha}{3} + \sqrt{\frac{6\gamma - 2\alpha}{9}} \cos\left(\delta + \frac{2\pi}{3}\right) \quad (4.46)$$

$$r = \sqrt{\frac{9}{6\gamma - 2\alpha}} \left[\beta + \frac{1}{54} \alpha (9\gamma - 5\alpha^2) \right]$$

$$\delta = \begin{cases} \frac{\pi}{3} & \text{for } r \leq -1 \\ 0 & \text{for } r \geq 1 \\ \arccos(r) & \text{for } -1 < r < 1 \end{cases}$$

The eigenvalues are named in such a way that $l_1 \geq l_2 \geq l_3$ and thus $l_3 = m_h^2$, whereas l_1 and l_2 correspond to the masses of the scalars ϕ_1 and ϕ_2 .

4.3.4 Thermal masses of the adjoint fSU(N)cSM

Using Equations (2.22) and (2.24) one can now write down the general thermal mass contributions. First, for the gauge self-energy one needs to determine $C_2(r), N_s$ and N_f . For this model, there are $N^2 - 1$ real scalar degrees of freedom in the hidden sector, i.e. $N_s = N^2 - 1$. N_f is simply given by:

$$N_f = N(\text{spin})(\text{particle/anti-particle}) = 4N \quad (4.47)$$

Lastly, the quadratic Casimir invariant for the adjoint representation of $SU(N)$ is simply $C_2(A_{SU(N)}) = N$. Together, this yields:

$$m_{X,\text{thermal}}^2(T) = \frac{2N + 2N + \frac{N^2-1}{4}}{6} g_X^2 T^2 = \frac{N^2 + 16N - 1}{24} g_X^2 T^2 \quad (4.48)$$

The scalar thermal mass contributions have besides the self-interaction terms λ_i also interaction between the hidden and visible sector. For the SM Higgs, the total contribution is:

$$m_{h,\text{thermal}}^2(T) = \left(\frac{1}{2} \lambda_1 + \frac{N^2 - 1}{12} \lambda_2 + \frac{3}{16} g^2 + \frac{1}{16} g'^2 + \frac{N}{12} y_t^2 \right) T^2 \quad (4.49)$$

And finally, for the scalars in the hidden sector:

$$m_{\phi,\text{thermal}}^2(T) = \left(\frac{1}{2} (\lambda_3 + \lambda_4) + \frac{1}{12} \lambda_2 + \frac{N}{4} g_X^2 + \frac{N}{3} y_X^2 \right) T^2 \quad (4.50)$$

The thermal masses of the scalars is then obtained by diagonalizing the total mass matrix, which is simply the Hessian, as defined in Equation (4.22), with an added diagonal matrix with the terms in Equations (4.49) and (4.50) on the diagonal. In further calculations, the diagonalization and calculation of corresponding eigenvalues is done numerically with CosmoTransitions (see Chapter 6), so no explicit formulas are given for the eigenvalues.

4.4 The MfSU(N)cSM

The second model will turn out to be more generally calculable. This model also has a $SU(N)$ gauge group, but with the more 'standard' fundamental representation for the scalar field Φ . In addition a complex scalar singlet $\sigma = \sigma_1 + i\sigma_2$ interacts with Φ and is coupled to N_f Majorana fermions with coupling strength Y_{ij} . This model is similar to the model discussed in [14] with the main difference that they identify the Majorana fermions as right-handed neutrino's and thus include a Yukawa coupling with the SM.

The singlet could explain the small masses of light-handed neutrino's via the type I or type II seesaw mechanisms [87, 88]. So studying this combination has renewed interest in the past years in extensions of the SM [89, 90]. In this model there are again $N^2 - 1$ new gauge bosons. The model will be referred to as the MfSU(N)cSM to exemplate the Majorana fermions it contains. The MfSU(N)cSM has the following tree-level potential:

$$V^{(0)} = \lambda_1(H^\dagger H)^2 + \lambda_2(H^\dagger H)(\Phi^\dagger \Phi) + \lambda_3(\Phi^\dagger \Phi)^2 + \lambda_4(\Phi^\dagger \Phi)|\sigma|^2 + \lambda_5|\sigma|^4 \quad (4.51)$$

This model has seven new parameters ($\lambda_1, \lambda_2, \lambda_3, \lambda_4, \lambda_5, g_X$ and Y_{ij}), where again two can be fixed. So this means the model has five free parameters and the two general choices of N and N_f . To constrain this freedom, N_f will be set to three in this thesis, as it is the minimum number of fermion families needed to introduce CP-violating terms in the CKW-matrix Y_{ij} .¹⁰ However, for simplicity the matrix is taken to be diagonal and $Y_{ii} = Y$ during the numerical calculations in the following chapters. Again the global symmetries of the effective potential are used to write the tree-level potential fully in terms of radial fields h, ϕ and σ :

$$V^{(0)} = \frac{\lambda_1}{4}h^4 + \frac{\lambda_2}{4}h^2\phi^2 + \frac{\lambda_3}{4}\phi^4 + \frac{\lambda_4}{4}\phi^2\sigma^2 + \frac{\lambda_5}{4}\sigma^4 \quad (4.52)$$

4.4.1 Mass eigenvalues

Similar to the adjoint fSU(N)cSM the Hessian is now calculated for the tree-level potential. This yields five different terms:

$$\frac{\partial^2 V^{(0)}}{\partial h_a \partial h_b} = \delta_{ij} \left[\lambda_1 h^2 + \frac{\lambda_2}{2} \phi^2 + 2\delta_{a4} \lambda_1 h^2 \right] \quad (4.53)$$

$$\frac{\partial^2 V^{(0)}}{\partial \phi_a \partial \phi_b} = \delta_{ab} \left[\lambda_3 \phi^2 + \frac{\lambda_2}{2} h^2 + \frac{\lambda_4}{2} \sigma^2 + 2\delta_{a(2N+4)} \lambda_3 \phi^2 \right] \quad (4.54)$$

$$\frac{\partial^2 V^{(0)}}{\partial \sigma_a \partial \sigma_b} = \delta_{ab} \left[\lambda_5 \sigma^2 + \frac{\lambda_4}{2} \phi^2 + 2\delta_{i2} \lambda_5 \sigma^2 \right] \quad (4.55)$$

$$\frac{\partial^2 V^{(0)}}{\partial h_a \partial \phi_b} = \delta_{a4} \delta_{b(2N)} \lambda_2 \phi h \quad (4.56)$$

$$\frac{\partial^2 V^{(0)}}{\partial \phi_a \partial \sigma_b} = \delta_{a(2N)} \delta_{b2} \lambda_4 \phi \sigma \quad (4.57)$$

Here the indices a, b run from $1, \dots, 4/1, \dots, 2N/1, 2$ for h, ϕ and σ , respectively. This means the Hessian matrix is diagonal, except for a 3×3 -block for every possible value of N . This makes this model excellent to study analytically as the same algorithm as for the $N = 2$ case for the adjoint fSU(N)cSM can be used, as given in Equations (4.44)

to (4.46). However, α, β and γ are now defined for the matrix $M = \begin{pmatrix} A & B & 0 \\ B & C & D \\ 0 & D & E \end{pmatrix}$:

¹⁰As discussed in Section 3.2.

$$\begin{aligned}
\alpha &= A + C + E \\
\beta &= ACE - D^2A - B^2E \\
\gamma &= A^2 + C^2 + E^2 + 2(B^2 + D^2) \\
&\text{with} \\
A &= 3\lambda_1 h^2 + \frac{\lambda_2}{2} \phi^2 \\
B &= \lambda_2 h \phi \\
C &= 3\lambda_3 \phi^2 + \frac{\lambda_2}{2} h^2 + \frac{\lambda_4}{2} \sigma^2 \\
D &= \lambda_4 \phi \sigma \\
E &= 3\lambda_5 \sigma^2 + \frac{\lambda_4}{2} \phi^2
\end{aligned} \tag{4.58}$$

This gives three masses of scalar particles. Then there are the three SM Goldstone bosons as given in Equation (4.25). Different from the adjoint fSU(N)cSM is that there are now $2N$ extra Goldstone bosons with masses¹¹:

$$m_{G_\phi}^2(h, \phi, \sigma) = \frac{\lambda_2}{2} h^2 + \lambda_3 \phi^2 + \frac{\lambda_4}{2} \sigma^2 \tag{4.59}$$

$$m_{G_\sigma}^2(\phi, \sigma) = \frac{\lambda_4}{2} \phi^2 + \lambda_5 \sigma^2 \tag{4.60}$$

Furthermore, there are the masses of the X-bosons and the Majorana fermions:

$$m_X^2(\phi) = \frac{g_X^2}{4} \phi^2 \tag{4.61}$$

$$m_\psi^2(\sigma) = \frac{Y^2}{4} \sigma^2 \tag{4.62}$$

As discussed in Section 4.2, the Goldstone bosons will be neglected in the next chapters when the phase transition is studied.

Thermal mass corrections

The thermal mass corrections for this model are given straightforwardly from Equations (2.22) and (2.24), keeping in mind that Majorana fermions have a factor of $\frac{1}{2}$, but are not gauged in this model:

$$m_{X,\text{thermal}}^2(T) = \frac{2N + N/4}{6} g_X^2 T^2 = \frac{3N g_X^2 T^2}{8} \tag{4.63}$$

$$m_{h,\text{thermal}}^2(T) = \left(\frac{1}{2} \lambda_1 + \frac{1}{6} \lambda_2 + \frac{3}{16} g^2 + \frac{1}{16} g'^2 + \frac{N}{12} y_t^2 \right) T^2 \tag{4.64}$$

$$m_{\phi,\text{thermal}}^2(T) = \left(\frac{1}{2} \lambda_3 + \frac{1}{12} (\lambda_2 + \lambda_4) + \frac{N}{4} g_X^2 \right) T^2 \tag{4.65}$$

$$m_{\sigma,\text{thermal}}^2(T) = \left(\frac{1}{2} \lambda_5 + \frac{1}{12} \lambda_4 + \frac{N_f}{12} Y^2 \right) T^2 \tag{4.66}$$

So now the complete mass spectrum is known for the discussed models and it becomes possible to study the electroweak phase transition for each of them. Before any numerical analysis is done, the electroweak phase transition is studied in more detail in the next chapter.

¹¹Note that there are $2N - 1$ G_ϕ Goldstone bosons and 1 G_σ Goldstone boson.

Chapter 5

The electroweak phase transition

As has been already claimed earlier in this thesis, conformal extensions of the SM typically predict strong first-order electroweak phase transitions at high temperatures. To better understand why this happens and what the consequences are, the electroweak phase transition is studied in this chapter. First the mechanism of the phase transition in the early Universe is studied. Second, the ultimately measurable effect of this phase transition is examined, which is the production of gravitational waves.

5.1 Theoretical framework of bubble nucleation

To analyze bubble nucleation, one needs a proper description of the phase transition and all the relevant temperatures. First, a short description is given of the phase transition itself. Next the important temperatures are examined in more detail and a discussion is given of how to find these temperatures.

At very high temperatures, the complete Universe will be in its symmetric state. As this is also the groundstate of the effective potential, this is a stable configuration. However, the Universe will cool down while expanding and at some point a new local minimum will start to form at a non-zero field value. At some point, the critical temperature T_c , this minimum will become degenerate with the minimum at the origin and for lower temperatures will even become the global minimum. For $T < T_c$, for particles in the local minimum (the false vacuum) it will become energetically favorable to tunnel to the true vacuum. The particle will tunnel at some point and a bubble of true vacuum nucleates in the sea of false vacuum. However, the temperature corrections discussed in Chapter 2 yield cubic terms in terms of the scalar field ($\sim \phi^3$), which induces a barrier between the two minima. Furthermore, conformal models typically have minima that are very far apart [91]. These two facts make tunneling difficult for temperatures close to the critical temperature.

One can describe the probability of this tunneling by solving the equation of motion of a scalar particle ϕ . At zero temperature this can be done with quantum field theory and the probability of tunneling per unit time per volume is given up to some prefactor by [92]:

$$\Gamma(T) \sim \left(\frac{S_4(\phi)}{2\pi} \right)^2 e^{-S_4(\phi)} \quad (5.1)$$

where S_4 is the Euclidean action for the solution of the equations of motion:

$$S_4(\phi) = \int d^4x \left[\frac{1}{2} \left(\frac{d\phi}{dt} \right)^2 + \frac{1}{2} (\nabla\phi)^2 + V(\phi, 0) \right] \quad (5.2)$$

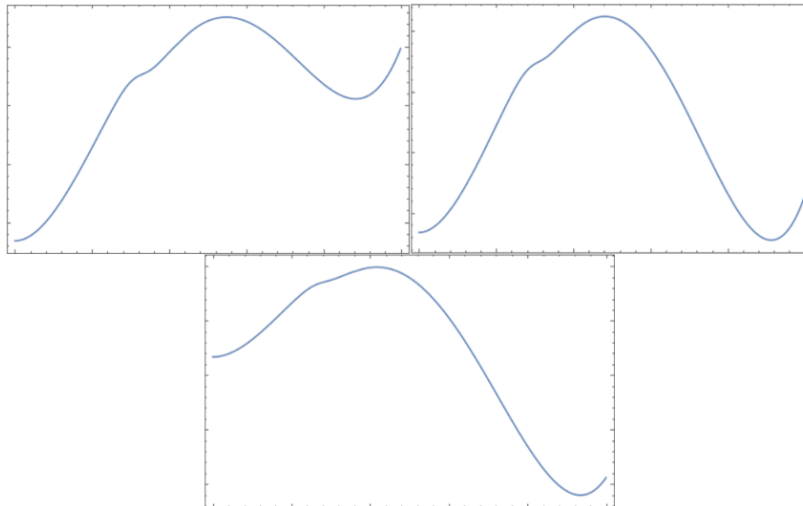


Figure 5.1: Development of the symmetry-breaking minimum. The vertical axis is the effective potential plotted for the field-value horizontally. For high-temperatures (left) the symmetric minimum is the global minimum, but there exists an unstable minimum at non-zero field value. At the critical temperature (right) the minima have become degenerate. Bottom shows the bubble nucleation phase, where particles can still be in the, now unstable, minimum at the origin. Through quantum or thermal fluctuations, the particle can tunnel through the barrier to the global minimum and a true vacuum bubble will nucleate.

Equation (5.1) gives the probability of tunneling by quantum fluctuations. However, as the Universe is at a finite temperature, thermal fluctuations are also able to induce tunneling. The integration over time, which as one remembers from Section 2.3, is now an integration over temperature, yielding simply a factor T^{-1} . By replacing $S_4(\phi) \rightarrow S_3(\phi)T^{-1}$ in Equation (5.1), one has the tunneling probability induced by thermal fluctuations:

$$\Gamma(T) \sim T^4 \left(\frac{S_3(\phi)}{2\pi T} \right)^{3/2} e^{-S_3(\phi)/T} \quad (5.3)$$

where the non-displayed prefactor has also produced a term T^3 in TFT. Again, ϕ is the solution to the equations of motion for the now three-dimensional action. These equations of motion can be generally given by:

$$\frac{d^2\phi}{dr^2} + \frac{d-1}{r} \frac{d\phi}{dr} = \frac{dV_{\text{eff}}(\phi, 0)}{d\phi} \quad (5.4)$$

where d is defined as the dimension of the action $S_d(\phi)$ and r is the radial coordinate in d -dimensional Euclidean space. In Section 5.1.1 it will be discussed that at some temperature, the nucleation temperature T_n , enough bubbles of true vacuum nucleate to keep up with the expansion of the Universe. This does not necessarily mean that the complete Universe will phase transition to the true vacuum, but generally, T_n is considered as the start of the phase transition. As the temperature decreases further, more and more bubbles will nucleate up to the point that from hydrodynamics one can say with certainty that the whole Universe will become filled with the true vacuum. This is the percolation temperature T_p and it will be discussed in Section 5.1.2.

The phase transition naturally generates a lot of energy, as due to the barrier and the widespread minima, the potential energy difference between the false and true vacuum is very large for conformal extensions. This is parametrized by the variable α , which measures the released energy ΔV relative to the total radiation energy present in the vacuum ρ_R :

$$\alpha \equiv \frac{\Delta V}{\rho_R} \quad (5.5)$$

For conformal extensions, such as discussed in this thesis, $\alpha \gg 1$. This energy is transferred to the plasma present in the early Universe, partially in terms of heat (exact details are given in Section 5.2. For large α , this means the Universe will reheat to a temperature T_r in a short amount of time. The reheating temperature is discussed in Section 5.1.3. The T_p or the T_r signal the end of the phase transition. As the actual process is more complicated, all temperature scales are now discussed in further detail in the next sections. Then in the last section, the production of gravitational waves by the bubbles is analyzed.

5.1.1 Nucleation Temperature T_n

This thesis uses the derivation from [93] to calculate the nucleation temperature. One starts by considering the decay rate of the false vacuum, which is related to the tunneling probabilities defined in Equations (5.1) and (5.3):

$$\Gamma(T) \simeq \max \left[T^4 \left(\frac{S_3}{2\pi T} \right)^{\frac{3}{2}} e^{-S_3/T}, R_0^{-4} \left(\frac{S_4}{2\pi} \right)^2 e^{-S_4} \right] \quad (5.6)$$

Here S_3 and S_4 are the 3- and 4- dimensional Euclidean actions, which determine the decay rate by thermal and quantum fluctuations, respectively. R_0 is the typical size of the nucleating bubble. For high temperatures, the tunneling typically takes place through thermal fluctuations, so the *max*-function in Equation (5.6) is dropped and only the term for S_3/T is considered. Then one can define a nucleation temperature T_n at which one bubble nucleates per Hubble volume:

$$N(T_n) = \int_{T_n}^{T_c} \frac{dT}{T} \frac{\Gamma(T)}{H(T)^4} = 1 \quad (5.7)$$

The Hubble rate comes from the Friedmann equations, where one takes into account the cosmological constant contribution to the false vacuum as the vacuum energy density ρ_V and the radiation domination via the radiation energy density ρ_R :

$$H^2 = \frac{1}{3M_{pl}^2}(\rho_R + \rho_V) = \frac{1}{3M_{pl}^2} \left(\frac{T^4}{\xi_g^2} + \Delta V \right) = H_V^2(\chi^{-1} + 1) \quad (5.8)$$

$$H_V \equiv \frac{\Delta V}{3M_{pl}^2} \quad (5.9)$$

$$\xi_g \equiv \sqrt{30/(\pi^2 g_*)} \quad (5.10)$$

$$\chi \equiv \frac{\rho_V}{\rho_R} = \frac{\xi_g^2 \Delta V}{T^4} \quad (5.11)$$

Here $g_* = 106.75$ is the number of degrees of freedom, the Planck mass is given by $M_{pl} = 2.435 \times 10^{18}$ GeV and ΔV is the difference between the true and false vacua. The temperature T_V at which the vacuum energy is equal to the radiation energy is thus defined by:

$$\frac{T_V^4}{\xi_g^2} = \Delta V \quad (5.12)$$

One can now make the assumption that below T_V the vacuum energy dominates and radiation dominates for $T > T_V$, which yields two different Hubble rate regimes. At sufficiently low temperatures, it is also correct to assume that ΔV is temperature-independent.

$$H(T) = \begin{cases} H_R(T) & = \frac{T^2}{\sqrt{3}M_{pl}\xi_g}, & T > T_V \\ H_V & = \frac{T_V^2}{\sqrt{3}M_{pl}\xi_g}, & T < T_V \end{cases} \quad (5.13)$$

With all this, it is possible to determine the critical value $y = S_3/T$ (or S_4) for a given temperature. Filling in equations 5.6 and 5.13 in 5.7, the condition becomes for $T < T_V$:

$$\begin{aligned}
1 &= \frac{y^{\frac{3}{2}} e^{-y} 9M_{pl}^4 \xi_g^4}{(2\pi)^{\frac{3}{2}}} \left(\int_{T_V}^{T_c} \frac{dT'}{T'} T'^4 T'^{-8} + \int_T^{T_V} \frac{dT'}{T} T'^4 T_V^{-8} \right) \\
y^{-\frac{3}{2}} e^y &= \frac{9M_{pl}^4 \xi_g^4}{(2\pi)^{\frac{3}{2}}} \left(\int_{T_V}^{T_c} \frac{dT'}{T'^5} + T_V^{-8} \int_T^{T_V} dT' T'^3 \right) \\
&= \frac{9M_{pl}^4 \xi_g^4}{(2\pi)^{\frac{3}{2}}} \left(\frac{-1}{4} (T_c^{-4} - T_V^{-4}) + \frac{1}{4} T_V^{-8} (T_V^4 - T^4) \right) \\
&= \frac{9M_{pl}^4 \xi_g^4}{4(2\pi)^{\frac{3}{2}}} \left(\frac{2}{\Delta V \xi_g^2} - T_c^{-4} - \frac{T^4}{\Delta V^2 \xi_g^4} \right) \tag{5.14}
\end{aligned}$$

Obviously, for $T_V < T < T_c$ there is no vacuum energy contribution according to the assumption. And for $T > T_c$ the non-trivial minimum becomes a local minimum and eventually disappears. So for all regimes, the condition becomes:

$$y^{-\frac{3}{2}} e^y = \begin{cases} \frac{9M_{pl}^4 \xi_g^4}{4(2\pi)^{\frac{3}{2}}} \left(\frac{2}{\Delta V \xi_g^2} - T_c^{-4} - \frac{T^4}{\Delta V^2 \xi_g^4} \right), & \text{for } 0 < T < T_V \\ \frac{9M_{pl}^4 \xi_g^4}{4(2\pi)^{\frac{3}{2}}} (T^{-4} - T_c^{-4}), & \text{for } T_V < T < T_c \\ 0, & \text{for } T > T_c \end{cases} \tag{5.15}$$

This yields the following plot:

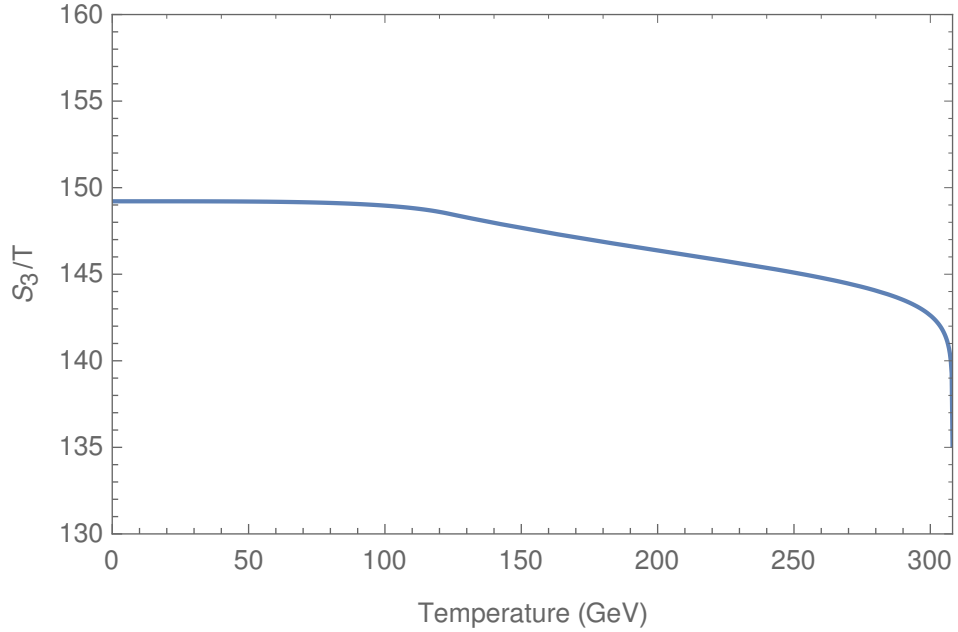


Figure 5.2: The critical value for S_3/T plotted as a function of temperature. For $T < T_V \approx 124$ GeV, the function is nearly constant.

5.1.2 Percolation temperature T_p

Another important quantity during bubble nucleation, is the percolation temperature T_p , which is the temperature where enough of space is filled by true vacuum bubbles to successfully complete the phase transition. Formally, it is the temperature at which enough bubbles overlap that a long-range connectivity is possible. One can assume that this is

therefore the temperature at which the phase transition ends. In a radiation-dominated Universe, this critical temperature is given by the demand that the volume fraction converted to the true vacuum $I(T_p) = 0.34$. Here 0.34 is the critical ratio between the volume of equal-sized, randomly-distributed and possibly overlapping spheres and the total volume of Euclidean space (in three dimensions) for which percolation occurs [94].

$I(T)$ is generally given by an expression in terms of the decay rate $\Gamma(T)$ and the scaled comoving size of a bubble $a(T)r(T, T')$:

$$I(t) = \frac{4\pi}{3} \int_T^{T_c} \frac{dT'}{T'H(T')} \Gamma(T') a(T')^3 r(T, T')^3 \quad (5.16)$$

The comoving size $r(T, T')$ with $T' > T$ is simply given by:

$$r(T, T') = \int_T^{T'} \frac{v_w d\tilde{T}}{\tilde{T}H(\tilde{T})a(\tilde{T})} = \int_T^{T'} \frac{d\tilde{T}}{\tilde{T}H(\tilde{T})a(\tilde{T})} = \int_T^{T'} \frac{d\tilde{T}}{H(\tilde{T})} \quad (5.17)$$

Here the general assumption is made that the bubble wall velocity v_w is close to 1 and using furthermore that the scale factor goes as $a(T) \sim T^{-1}$. Then the volume fraction converted to the true vacuum is:

$$I(T) = \frac{4\pi}{3} \int_T^{T_c} \frac{dT' \Gamma(T')}{T'^4 H(T')} \left(\int_T^{T'} \frac{d\tilde{T}}{H(\tilde{T})} \right)^3 \quad (5.18)$$

However, as was mentioned in section 5.1.1, during bubble nucleation the Universe cannot be assumed to always be radiation-dominated. For $T > T_V$, vacuum contributions must be taken into account. For $I(T)$ a second distinction must be made, which is that bubbles can nucleate during radiation domination and keep on growing into vacuum domination. So the equations for the different regimes (R , V and RV for radiation-, vacuum- and radiation-to-vacuum domination, respectively) are, using 5.13:

$$r_R(T, T') = \sqrt{3} M_{pl} \xi_g \left(\frac{1}{T} - \frac{1}{T'} \right) \quad (5.19)$$

$$r_V(T, T') = \frac{\sqrt{3} M_{pl} \xi_g}{T_V^2} (T' - T) \quad (5.20)$$

$$\begin{aligned} r_{RV}(T, T') &= \int_{T_V}^{T'} \frac{d\tilde{T}}{H_R(\tilde{T})} + \int_T^{T_V} \frac{d\tilde{T}}{H_V} \\ &= \sqrt{3} M_{pl} \xi_g \left(\frac{1}{T_V} - \frac{1}{T'} + \frac{T_V - T}{T_V^2} \right) \\ &= \sqrt{3} M_{pl} \xi_g \left(\frac{2}{T_V} - \frac{1}{T'} - \frac{T}{T_V^2} \right) \end{aligned} \quad (5.21)$$

And similarly one finds from 5.18 the volume fraction $I(T)$ for different growth regimes of the bubbles under the assumption that the decay rate is dominated by thermal fluctuations:

$$\begin{aligned}
I_R(T) &= \frac{4\pi}{3} \int_T^{T_c} \sqrt{3} M_{pl} \xi_g \frac{dT'}{(2\pi)^{\frac{3}{2}} T'^2} \left(\frac{S_3}{T'}\right)^{\frac{3}{2}} e^{-S_3/T'} \left(\sqrt{3} M_{pl} \xi_g \left(\frac{1}{T} - \frac{1}{T'}\right)\right)^3 \\
&= \sqrt{18/\pi} (M_{pl} \xi_g)^4 \int_T^{T_c} dT' \left(\frac{S_3}{T'}\right)^{\frac{3}{2}} e^{-S_3/T'} \left(\frac{1}{T} - \frac{1}{T'}\right)^3 \quad (5.22)
\end{aligned}$$

$$\begin{aligned}
I_{RV}(T) &= \frac{4\pi}{3} \left(\int_{T_V}^{T_c} \frac{dT' \Gamma(T')}{T'^4 H_R(T')} r_{RV}^3(T, T') + \int_T^{T_V} \frac{dT' \Gamma(T')}{T'^4 H_V(T')} r_V^3(T, T') \right) \\
&= \sqrt{18/\pi} (M_{pl} \xi_g)^4 \left(\int_{T_V}^{T_c} dT' \left(\frac{S_3}{T'}\right)^{\frac{3}{2}} e^{-S_3/T'} \left(\frac{2}{T_V} - \frac{1}{T'} - \frac{T}{T_V^2}\right)^3 + \right. \\
&\quad \left. \int_T^{T_V} dT' \left(\frac{S_3}{T'}\right)^{\frac{3}{2}} e^{-S_3/T'} \left(\frac{T' - T}{T_V^2}\right)^3 \right) \quad (5.23)
\end{aligned}$$

Since $I_R(T)$ is only applicable in the case that $T_n > T_V$, which is not the case for the models in this thesis, only $I_{RV}(T)$ is used and denoted as $I(T)$. So the percolation temperature can be found with the following condition:

$$I(T_p) = n_c = 0.34 \quad (5.24)$$

It must be noted that for temperatures lower than the percolation temperature, $I(T)$ is no longer correct. As after the percolation temperature is reached, it is assumed that the phase transitions ends and the Universe starts reheating due to the released energy during the phase transition. This will be discussed in the next section.

5.1.3 Reheating temperature T_r

The exact details of how reheating takes place are not of great importance, as long as one can assume that the reheating happened fast [93]. The reheating starts as soon as bubbles start to collide. The collision energy is then transferred to the plasma, which heats up (see Section 5.2.1). The reheating temperature depends on the total released energy as follow:

$$T_r = T_p (1 + \alpha(T_p))^{\frac{1}{4}} \quad (5.25)$$

As will be explained in the next section, it is of importance at which temperature the Universe ends bubble nucleation. As has been shown here, for phase transitions with $\alpha \gg 1$, such as the SU(2)cSM, nucleation ends at T_r . Note that most literature use that the end of the phase transition is at percolation temperature T_p . Furthermore, reheating can be of importance for baryogenesis [95]. As this is outside the scope of this thesis, this is not further discussed, but it is interesting to note. Now all the relevant temperatures are discussed, one can turn to the dynamics of bubbles, with in particular bubble collisions and the resulting production of gravitational waves.

5.2 Bubble hydrodynamics

The nucleation and expansion of bubbles of true vacuum are enough to describe the dynamics of a phase transition. However, single spherical bubbles are not able to produce gravitational waves, as follows from Birkhoff's theorem: spherical objects can be considered as point-like in terms of gravitational field for an external observer. So a growing spherical bubble is for the observer the same static object and cannot produce changes in the gravitational field. The assumption that the bubble starts spherical and stays spherical is justified by its large semiclassical action and surface tension [15].

This means one has to consider processes which arise during bubble collisions. These will be able to generate gravitational waves. The parameters of interest during these collisions are the speed of the bubble wall v_w and the ratio of the vacuum energy density

released to that of the total radiation energy in the plasma, called the latent heat α , introduced in Equation (5.5). It can be written in terms of the the potential energy difference between the true and false vacuum ΔV as introduced in Equation (5.11):

$$\alpha = \frac{\rho_V}{\rho_R} = \frac{\Delta V \xi_g^2}{T^4} \quad (5.26)$$

Furthermore, part of the vacuum energy gets converted into kinetical energy of the fluid and into gradient energy of the extra scalar field. The ratios of these are denoted by κ_v and κ_ϕ , respectively. In this thesis, the bubble wall velocity $v_w \approx 1$ as the fields involved in the phase transition (i.e. the new scalar fields) are typically weakly coupled to the SM particles in the plasma and therefore perceive little 'friction' from the hot plasma during bubble growth.

The last important parameter is the average time scale of the phase transition per Hubble time: β/H_* . One can easily see from Equation (5.1) that β can indeed be interpreted as the transition time scale:

$$\Gamma(t) \sim e^{-\beta t} \quad (5.27)$$

The timescale is the time between the start of the phase transition T_n and the end of the phase transition, typically defined to be at T_p . If one assumes a quick phase transition ($T_n \approx T_p$), the timescale is given by:

$$\frac{\beta}{H_*} = T_p \left. \frac{d(S_3/T)}{dT} \right|_{T=T_p} \quad (5.28)$$

This definition will be used in the next chapter for the numerical calculations. One can distinguish three different processes that contribute to the production of gravitational waves:

- Bubble wall collisions
- Propagation (and dissipation) of soundwaves through the plasma after collision
- Turbulence

The three contributions will be explained further in the next sections, but for now one can state that the expected measured energy in gravitational waves $h^2\Omega_{\text{GW}}$ for a certain frequency f is given by [96]:

$$h^2\Omega_{\text{GW}} \simeq h^2\Omega_{\text{coll}} + h^2\Omega_{\text{sw}} + h^2\Omega_{\text{turb}} \quad (5.29)$$

5.2.1 Bubble collisions

The gravitational energy released during bubble collisions is from the scalar field involved in the phase transition. To compute its contribution, the 'envelope approximation' is used (see [96] and references therein for a complete description). It assumes that a fraction κ_ϕ of the energy is stored in a shell around the bubble walls. After collision, the energy quickly dissipates away, so one can approximate that all the envelope energy is in yet-to-collide bubble shells. Then one can calculate its contribution with numerical simulations, which is given by:

$$h^2\Omega(f) = 1.67 \cdot 10^{-5} \left(\frac{H_*}{\beta} \right)^2 \left(\frac{\kappa_\phi \alpha}{1 + \alpha} \right)^2 \left(\frac{100}{g_*} \right)^{\frac{1}{3}} \left(\frac{0.11 v_w^3}{0.42 + v_w^2} \right) S_{\text{env}}(f) \quad (5.30)$$

$$S_{\text{env}}(f) = \frac{3.8(f/f_{\text{env}})^{2.8}}{1 + 2.8(f/f_{\text{env}})^{3.8}}$$

$$f_{\text{env}} = \left(\frac{0.62}{1.8 - 0.1v_w + v_w^2} \right) \left(\frac{\beta}{H_*} \right) h_*$$

where h_* is the inverse Hubble time at time t_* of the GW production redshifted to today. However, for models with massive vector bosons, as the models discussed in this thesis, the contribution from bubble collisions is negligible [97]. These gauge bosons source a friction term that prevents runaway bubbles¹ (although it is still safe to assume $v_w \approx 1$) and accumulate energy in their shells. So for this thesis, the contribution from bubble collisions is not considered for determining gravitational wave spectra.

5.2.2 Soundwaves

Percolation of bubbles also produces motion in the plasma with a factor of κ_v . This motion propagates through the plasma in the form of sound waves. Again one can find an expression for the contribution to gravitational waves by considering numerical simulations, albeit very difficult [98]. Acoustic production of gravitational waves is still heavily researched and especially for strong phase transitions (i.e. $\alpha \gg 1$). Current numerical fits are given by [91]:

$$\begin{aligned} h^2 \Omega_{\text{sw}}(f) &= 2.65 \cdot 10^{-6} \left(\frac{H_*}{\beta} \right) \left(\frac{\kappa_v \alpha}{1 + \alpha} \right)^2 \left(\frac{100}{g_*} \right)^{\frac{1}{3}} v_w S_{\text{sw}}(f) \quad (5.31) \\ S_{\text{sw}}(f) &= (f/f_{\text{sw}})^3 \left(\frac{7}{4 + 3(f/f_{\text{sw}})^2} \right)^{7/2} \\ f_{\text{sw}} &= 1.9 \cdot 10^{-2} \text{mHz} \frac{1}{v_w} \left(\frac{\beta}{H_*} \right) \left(\frac{T_*}{100 \text{ GeV}} \right) \left(\frac{g_*}{100} \right)^{1/6} \end{aligned}$$

For strong phase transitions, the dependence on α drops out. The peak frequency f_{sw} is related to the main scale of the transition, which is the average bubble separation $R_* = (8\pi)^{\frac{1}{3}} v_w / \beta$. Equations (5.30) and (5.31) differ roughly by a factor of β/H_* , which is due to the fact that soundwaves contribute as a long-lasting source, generating gravitational waves well after collisions have taken place, whereas collisions are more or less instantaneous. This again justifies that soundwaves are a more dominant contribution to the gravitational wave spectra than bubble collisions. The temperature T_* is the temperature after collision, which one can identify as the reheating temperature.

5.2.3 Turbulence

The third contribution is induced by turbulence in the plasma. As the plasma is fully ionized at GeV-temperatures, the main factor of turbulence is through magnetohydrodynamics (MHD). Just as for soundwaves, this is a long-lasting contribution, as one can see in its contribution to the spectrum:

$$\begin{aligned} h^2 \Omega_{\text{turb}}(f) &= 3.35 \cdot 10^{-4} \left(\frac{H_*}{\beta} \right) \left(\frac{\kappa_{\text{turb}} \alpha}{1 + \alpha} \right)^{\frac{3}{2}} \left(\frac{100}{g_*} \right)^{\frac{1}{3}} v_w S_{\text{turb}}(f) \quad (5.32) \\ S_{\text{turb}}(f) &= \frac{(f/f_{\text{turb}})^3}{(1 + (f/f_{\text{turb}}))^{\frac{11}{3}} (1 + 8\pi f/h_*)} \\ f_{\text{turb}} &= 2.7 \cdot 10^{-2} \text{mHz} \frac{1}{v_w} \left(\frac{\beta}{H_*} \right) \left(\frac{T_*}{100 \text{ GeV}} \right) \left(\frac{g_*}{100} \right)^{1/6} \end{aligned}$$

where κ_{turb} is the fraction of latent heat transformed into MHD turbulence. The main difference with the soundwaves contribution is the exponent for κ . It is found that the dominant contribution is still from soundwaves, but for off-peak frequencies, turbulence might start to dominate [91]. For this thesis, models with $v_w \approx 1$, $\alpha \gg 1$ and no runaway bubbles are studied and thus only contributions from soundwaves, as defined in Equation (5.31) are considered:

$$h^2 \Omega_{\text{GW}}(f) = h^2 \Omega_{\text{sw}}(f) \quad (5.33)$$

¹Accelerating bubbles are typically called runaway bubbles.

However, for other types of models with different features of the phase transition the contributions might be related differently and careful consideration is needed.

In conclusion, for this thesis only the production of gravitational waves from sound-waves is considered. These are long-lasting and, as can be seen from Equation (5.31), are mainly dependent on the strength and duration of the phase transition, as characterized by the quantities α and β/H_* . Now all theoretical issues surrounding conformal extensions are discussed and in the next chapter, numerical results can be computed.

Chapter 6

Numerical analysis

To study the electroweak phase transition described in Chapter 5 a numerical program is needed to determine the bounce solution and calculate the Euclidean action for a given temperature. Several programs exist at the moment, all with their advantages and disadvantages[30, 99–101]. For this thesis, CosmoTransitions will be used[30]. It is a Python-based script, which tries to analyze a given input theory (i.e. effective potential), find its minima for different temperatures and derive the characteristics of the corresponding (if present) phase transitions. Lastly, it finds the bubble wall profiles and critical Euclidean action. For this thesis, the code has been expanded to also determine the nucleation and percolation temperatures (as given in Section 5.1) as well as any emergent gravitational wave spectra (as was explained in Chapter 5).

The program as it now stands, is able to completely work through an input model and give all characteristics of importance in a matter of minutes, which makes it a fast and useful tool. As the papers this thesis continues on¹ used a different program (i.e. AnyBubble [100] for the tunneling calculations and [102] for the thermal functions), this chapter will provide some details of how CosmoTransitions works and the differences with AnyBubble.

6.1 The over- and undershoot method

The main objective of CosmoTransitions is to determine the bubble profile along the tunneling path and the corresponding critical Euclidean action, as has been explained in Section 5.1. If CosmoTransitions has found two minima at a certain temperature T , it tries to find a solution for the bubble's equations of motion. These are given by:

$$\frac{d^2 \vec{\phi}}{d\rho^2} + \frac{\alpha}{\rho} \frac{d\vec{\phi}}{d\rho} = \nabla V(\vec{\phi}) \quad (6.1)$$

Depending on if one is looking for tunneling at finite or zero temperature, $\alpha=2,3$ and $\rho^2 = r^2, r^2 - t^2$ respectively, where r is the spatial radial coordinate and t the time coordinate. Lastly, $\vec{\phi}$ is the vector which spans the scalar field space.

The equations of motion can be solved by the overshoot/undershoot method if the field is only one-dimensional. One can think of this procedure as trying to roll a classical particle on the inverted potential $-V(\phi)$. The particle starts at the global minimum ϕ_{glob} and rolls down to the local minimum ϕ_{loc} for growing ρ as depicted in Figure 6.1.

So ρ acts as some kind of time in this case. At $\rho \rightarrow \infty$ the particle should exactly stop at ϕ_{loc} as very far outside the bubble, one expects the vacuum to still be the false vacuum. If at $\rho \rightarrow \infty$ the particle over- or undershoots, the starting point was too close or too far. Numerically, this method can be repeated until the initial point ϕ_{tunnel} is

¹This thesis continues on the work of two previous papers [10, 15]

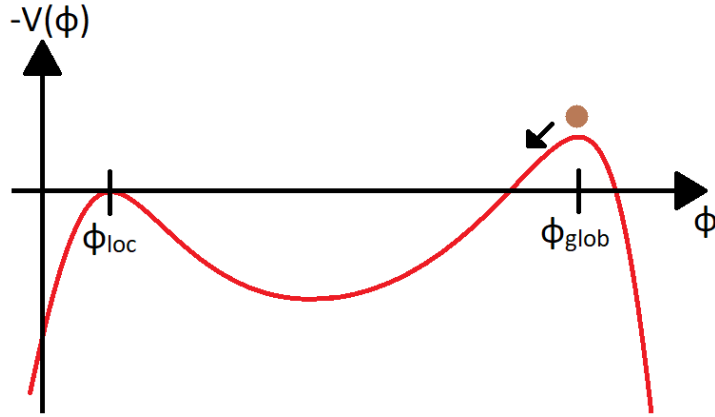


Figure 6.1: The overshoot/undershoot method for a fictive inverted potential. As the particle rolls down from the global minimum ϕ_{glob} (now a maximum), it tries to stop precisely at ϕ_{loc} .

found to arbitrary precision. This point ϕ_{tunnel} should be thought of the point as where the quantum particle appears again from under the barrier after which it rolls down further to the global minimum ϕ_{glob} . Then one can calculate the Euclidean action between ϕ_{tunnel} and ϕ_{loc} .

For multi-dimensional fields, the first step to solve the equations of motion are to reduce the problem to an one-dimensional one. This is done by guessing an initial path $\vec{\phi}_{\text{guess}}$ in field space with parametrization coordinate x along the path. Next the equations of motion are split into a parallel and a perpendicular direction:

$$\frac{d^2x}{d\rho^2} + \frac{\alpha}{\rho} \frac{dx}{d\rho} = \frac{\partial}{\partial x} V[\vec{\phi}(x)] \quad (6.2)$$

$$\frac{d^2\vec{\phi}}{dx^2} \left(\frac{dx}{d\rho} \right)^2 = \nabla_{\perp} V(\vec{\phi}) \quad (6.3)$$

The first equation of motion can be solved by the overshoot/undershoot method as it is the same as Equation (6.1). If $\vec{\phi}_{\text{guess}}$ was correct, then the solution for Equation (6.2) will also solve Equation (6.3). So now the path $\vec{\phi}_{\text{guess}}$ must be deformed until it does. This can be done by again thinking of this classically where $\vec{\phi}_{\text{guess}}$ is a fixed path along which a particle moves. As it rolls along the track, it will feel a force from the potential it is rolling through. Naturally, the parallel force (and thus the speed of the particle) is given by Equation (6.2) and the normal force trying to push it off the track is given by:

$$\vec{F}_{\text{norm}} = \frac{d^2\vec{\phi}}{dx^2} \left(\frac{dx}{d\rho} \right)^2 - \nabla_{\perp} V(\vec{\phi}) \quad (6.4)$$

By splitting up the path in smaller segments, each part can be deformed in the direction of \vec{F}_{norm} , forming a new path $\vec{\phi}$. This is repeated by the algorithm until the path solves both Equations (6.2) and (6.3), i.e. $\vec{F}_{\text{norm}} = 0$. From this, the Euclidean action can be calculated and used to determine the nucleation temperature.

6.2 Result for the benchmark model SU(2)cSM

As typically studying a phase transition numerically is very difficult for any numerical program, CosmoTransitions is first tested on the known phase transition of the SU(2)cSM. As will become clear, CosmoTransitions will yield different results than found before, underlining the difficulty of correctly studying phase transitions numerically. As a

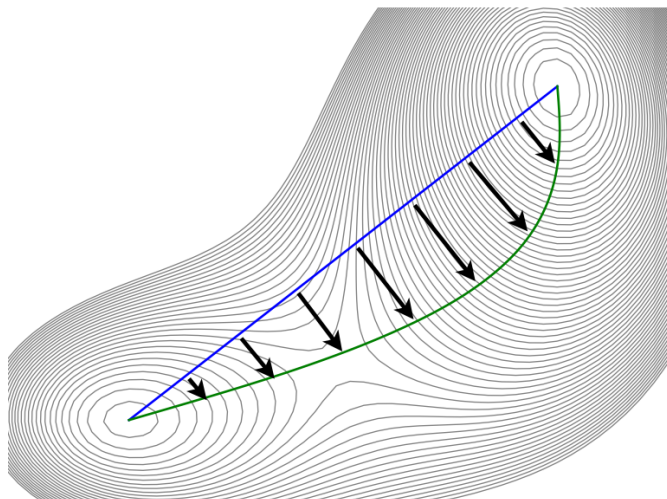


Figure 6.2: Schematic picture of the deformation of a tunneling path under influence of the underlying potential in two dimensions. The initial path (blue) is deformed in the direction of the true tunneling path (green) through the normal force exerted by the potential. Picture taken from [30].

guideline, the characteristic values found in [15] are calculated with the CosmoTransitions package. The values found in [15] are given in Table 6.1.

#	λ_1	λ_2	λ_3	g_X	v [GeV]	w [GeV]	T_c [GeV]	T_n [GeV]	β/H_*	α
1	0.175	-0.0049	-0.0038	0.83	246	2200	281	22	597	447
2	0.149	-0.0065	-0.0058	0.94	246	1774	256	27	319	213
3	0.119	-0.0013	-0.0136	1.01	246	3611	568	60	265	170
4	0.122	-0.0050	-0.0104	1.05	246	1860	302	34	297	137
5	0.166	-0.0083	-0.0063	0.97	246	1648	244	24	325	245
6	0.120	-0.0019	-0.0079	0.92	246	2991	428	39	418	345
7	0.124	-0.0030	-0.0047	0.85	246	2411	318	28	434	361
8	0.139	-0.0095	-0.0093	1.08	246	1426	236	28	234	115

Table 6.1: Table with parameters and characteristics of the phase transition in the $SU(2)_{cSM}$ for eight different benchmark points as found in [15].

They studied eight different benchmark points for the parameters and determined the VEV's at $T = 0$ (v and w), the critical and nucleation temperature T_c and T_n and lastly the typical strength of the transition and its duration, given by β/H_* and α , respectively. As has become clear from the discussion in Section 5.2, percolation and reheating temperature T_p and T_r are of bigger importance than previously thought. So these found values for the eight benchmark points are also presented in Section 6.2.1 along with the ones previously mentioned. In Section 6.2.2 benchmark point 7 is analysed and multiple plots are presented to better show the phase transition.

6.2.1 Results on benchmark points

The values found by CosmoTransitions are given in Table 6.2. One can quickly see that the values are very different from the ones in Table 6.1. Typically, the critical temperature T_c is of comparable values, but the nucleation temperature T_n is an order of magnitude smaller for the points analyzed in CosmoTransitions. As for lower temperatures, the global minimum becomes even steeper, naturally the found α is much bigger and the duration of the phase transition faster. And this also follows from the results. As this order of magnitude difference in the nucleation temperature is alarming, further inspection is needed to make sure that the results from CosmoTransitions are correct.

This will be done by analyzing benchmark point 7 in more detail in Section 6.2.2, just as was done in [15].

The reheating and percolation temperature have not been calculated before for the SU(2)cSM. Interestingly, for all benchmark points the percolation temperature is around half the nucleation temperature. This means that the phase transition is not instantaneous, but is completed in all cases and then reheating starts. A last remark must be made on benchmark point 1. Unfortunately, CosmoTransitions was not able to properly track the movement of the global minimum for different temperatures. From analyzing the potential it was found that benchmark point 1 should have a similar phase transition as the other benchmark points and this is thus no more than a numerical flaw from CosmoTransitions.

#	v [GeV]	w [GeV]	T_c [GeV]	T_n [GeV]	β/H_*	α	T_p [GeV]	T_r [GeV]
1	-	-	-	-	-	-	-	-
2	247.21	1774.79	247.80	3.62	41.61	$5.73 \cdot 10^5$	1.42	99.6
3	246.80	3599.17	516.70	16.05	41.48	$3.34 \cdot 10^4$	10.9	216.98
4	246.14	1849.60	283.96	15.62	50.59	$3.03 \cdot 10^3$	9.41	115.89
5	247.83	1651.91	237.19	4.87	41.74	$1.48 \cdot 10^5$	2.26	95.52
6	245.31	2973.51	400.18	3.73	33.17	$3.65 \cdot 10^6$	1.70	163.04
7	249.09	2430.76	308.15	0.74	26.79	$7.8 \cdot 10^8$.28	123.67
8	247.54	1426.52	226.23	16.96	57.27	$8.62 \cdot 10^2$	10.93	310.32

Table 6.2: The values found by CosmoTransitions for the eight benchmark points given in Table 6.1. New are the values for the percolation and reheating temperatures T_p and T_r . For benchmark point 1, CosmoTransitions was not able to analyze the phase transition.

6.2.2 Figures of benchmark point 7

As CosmoTransitions is not finding the same values for the phase transitions as AnyBubble, a closer look is needed into where this difference originates from. Perhaps the most difficult part of analyzing a phase transition numerically, is finding the correct critical tunneling action. So at what temperature does Equation (5.7) hold? This can be most easily studied by constructing a plot for the found tunneling action as a function of temperature. As this is also done in [15], the figures are compared in Figures 6.3 and 6.4. As this is very hard to do numerically, this might be a good starting point to compare the two.

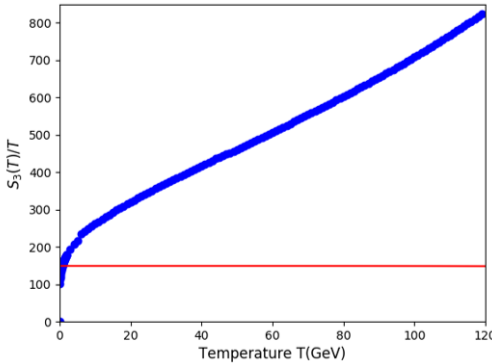


Figure 6.3: The tunneling action for the SU(2)cSM for benchmark point 7 as a function of temperature T as found by CosmoTransitions. The red line is the critical tunneling action as calculated by Equation (5.7).

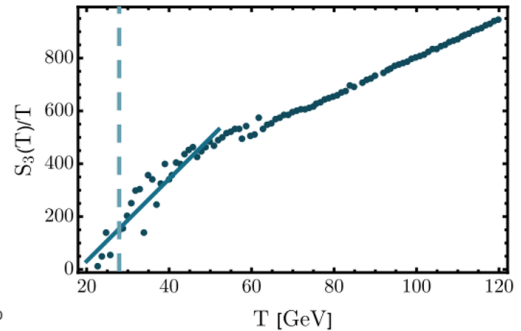


Figure 6.4: The tunneling action for the SU(2)cSM for benchmark point 7 as a function of temperature T as found by the AnyBubble program in [15]. A linear fit is done around T_n to estimate the value of β/H_* .

Now the difference becomes immediately clear. For temperatures smaller than ~ 50 GeV, AnyBubble clearly starts showing scattered points. For temperatures > 50 GeV the two plots match, so one would think that the smoother continuation of Figure 6.3 makes more sense. A possible explanation for the scattering of points found by AnyBubble is that for lower temperatures it becomes increasingly hard to numerically find the minimum at the origin. This has two reasons. First, as mentioned before, the global minimum becomes deeper and second, the barrier decreases for decreasing temperatures. So relatively, the minimum at the origin becomes increasingly shallow and thus harder to find for a numerical program. This could produce varying values of tunneling action as seen in Figure 6.4.

Therefore the conclusion is now that the results from CosmoTransitions are correct. As is seen in Table 6.2, the percolation and reheating temperatures have also been studied. Equation (5.24) yields a condition for bubble percolation as a function of temperature. The condition, along with the numerical values found for benchmark point 7 are shown in Figure 6.5.

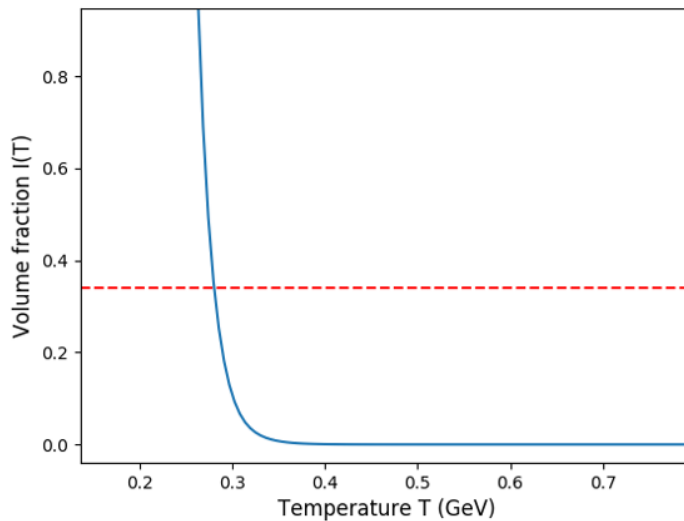


Figure 6.5: The volume fraction of the Universe inside bubbles of true vacuum $I(T)$ as a function of temperature T in blue. The red-dotted line is the critical fraction for percolation as explained in Section 5.1.2. For values below the percolation temperature, $I(T)$ is no longer correct as the Universe starts reheating.

In Figure 6.5 it seems as if $I(T)$ diverges for small temperatures, which should not be possible for a ratio. However, as stated before, $I(T)$ is not well-defined for $T < T_p$ as the Universe starts reheating after percolation. So the divergence should be ignored in this case.

The last figure of interest for benchmark point 7 is the actual tunneling trajectory during this phase transition. As has been explained in Section 6.1, CosmoTransitions finds the optimal tunneling path and this can be plotted on the potential. This has been done in Figure 6.6.

One sees that the tunneling takes place along the ϕ -direction. This is exactly the same as what was found in [15]. It should be noted that the particle actually tunnels under the barrier, where the black line in Figure 6.6 implies incorrectly that the particles moves over the barrier. This is just a graphical choice. After tunneling through the barrier, the scalar particle rolls down the potential to the global minimum.

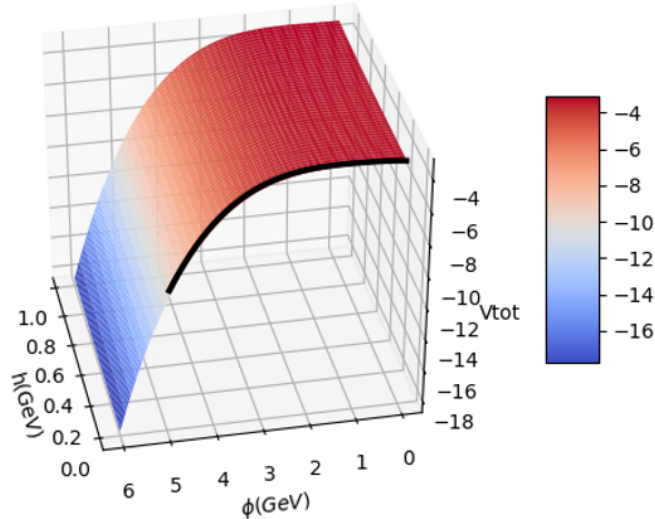


Figure 6.6: 3D-plot of the effective potential of the SU(2)cSM near the origin of the two scalar fields h and ϕ at the nucleation temperature $T_n = 0.74$ GeV. The black line is the tunneling path found by CosmoTransitions. The barrier at $\phi \approx 2$ GeV is barely visible, but is present.

6.2.3 The SGWB of the SU(2)cSM

Of course the final goal of introducing any conformal extension of the SM is to measure its gravitational wave background. The predicted SGWB for the SU(2)cSM was also shown in [15]. However, as all benchmark points turned out to have stronger and shorter phase transitions, one would expect also different SGWB's.

Furthermore, a new assumption is made with respect to the peak frequency f_{sw} in Equation (5.31). This frequency must be red-shifted to present day, but the red-shifting didn't start from the nucleation temperature, as assumed in [15]. The Universe reheated after the phase transition and the gravitational waves are expected to source from these temperatures. So red-shifting should be calculated from the reheating temperature until present day, instead of from the nucleation temperature. This means that in Equation (5.31) one should identify $T_* = T_r$.

Now computing the spectrum of gravitational waves produced by the electroweak phase transition yields the curves plotted in Figure 6.7. The spectra are well above the best² expected sensitivity range of LISA [103].³ All seven benchmark points are included in the figure, but not all are distinguishable from each other. Compared to [15], the SGWB's have stronger peaks at smaller frequencies. This is exactly what one would expect, as the phase transitions are found to be stronger, but the signals are more red-shifted as they come from higher temperatures.

6.3 Analysis of the adjoint fSU(2)cSM and MfSU(2)cSM

Even though the aim of this thesis is to stay as general as possible for the adjoint fSU(N)cSM and MfSU(N)cSM, one still is required to pick values for the six and seven parameters. As mentioned before, two of these parameters are fixed by the SM Higgs

²ESA has at the moment of writing not updated their expected sensitivity curves to account for the surprisingly strong results from LISA Pathfinder, so here the best sensitivity curve of the original requirements is used.

³Unfortunately, it is not possible to give a signal-to-noise ratio (SNR) for these spectra as the area between the background and detector curves is not trivially related to the SNR [104]. If one would compute the characteristic strain of the gravitational waves and plot them against the sensitivity curves, the area would correspond to the SNR. However, computing the characteristic strain was not part of this thesis and thus must be left for future research.

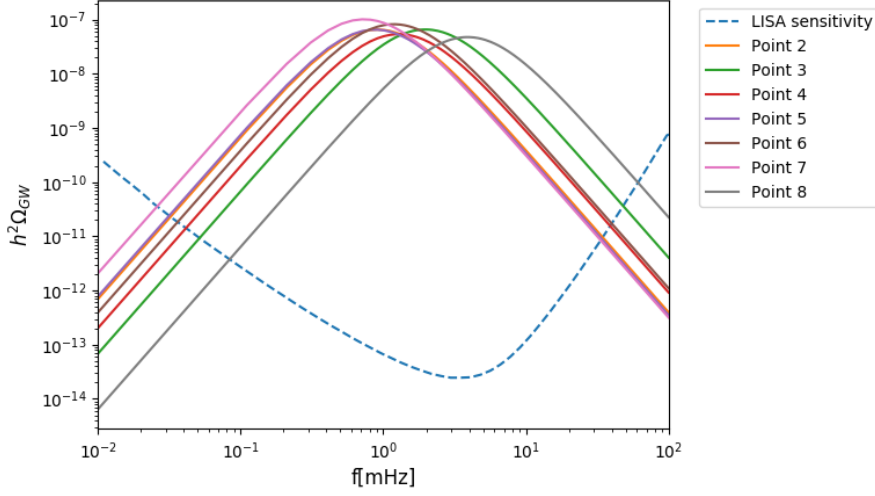


Figure 6.7: The stochastic gravitational wave backgrounds for different benchmark points of the SU(2)cSM. The expected sensitivity curve from LISA is also plotted (dashed line).

mass and VEV. Numerically, it is possible to check for these conditions in CosmoTransitions for different values of the parameters. This has been done in [10] for the SU(2)cSM. They also check for the running of the couplings and solve their RGE equations. Then one can also check the stability of the potential (as discussed in Section 3.3) at the Planck scale.

In the timespan of this thesis, it was not possible to implement these last two checks in CosmoTransitions. However, a scan of the parameter space has been done for the adjoint fSU(2)cSM and the MfSU(2)cSM with $N_f = 3$. The benchmark points found by CosmoTransitions are shown in Tables 6.3 and 6.4. From the results, it is clear that for very small deviations in the parameter values, large differences in the minima and Higgs mass were found. This made it hard to find very different benchmark points, as many million iterations must be performed to only find one set of points.

#	λ_1	λ_2	λ_3	λ_4	g_X	y_X	v [GeV]	w_{ϕ_1} [GeV]	w_{ϕ_2} [GeV]
1	0.17248	-0.5599	0.6111	-0.3325	0.7159	0.01	245.2	142.2	142.6
2	0.17237	-0.5620	0.6193	-0.3397	0.7189	0.01	246.1	143.0	143.0

Table 6.3: Two benchmark points for the adjoint fSU(2)cSM. For both points, the Yukawa coupling λ_f was set to 0.01 to simplify the parameter scan.

#	λ_1	λ_2	λ_3	λ_4	λ_5	g_X	Y	v [GeV]	w_ϕ [GeV]	w_σ [GeV]
1	0.11629	-0.012817	0.090752	-0.08775	0.02160	0.8810	0.01	246.4	1501	2314
2	0.11634	-0.012852	0.090720	-0.08784	0.02187	0.8815	0.01	241.2	332.7	471.7

Table 6.4: Two benchmark points for the MfSU(2)cSM. For both points, the Yukawa coupling Y was set to 0.01 to simplify the parameter scan.

Unfortunately, when analyzing the possible phase transitions in these models for the given benchmark points, no phase transitions were found. The numerical analysis of these phase transitions is very delicate. What is meant is that correct tracking of the minima for different temperatures, highly depends on correctly fine-tuning the multiple precision parameters of minimization procedures. This was also the case for the SU(2)cSM, where at least the benchmark points were already known to behave properly, so for these models

it is even more difficult. Due to the restriction of time for this thesis, it has therefore not been possible to analyze the introduced models on their symmetry-breaking and phase transitions. The expectation is that in future research this will be possible and that the symmetry-breaking patterns discussed in Section 4.1 will appear.

For now, the visualisations of the effective potential are discussed for the two models. First, the adjoint fSU(2)cSM. As the two new scalar fields ϕ_1 and ϕ_2 can be exchanged, without changing any of the expressions, one would expect that the potential is also symmetric along these two axes. This turns out to be indeed the case, so only the h - and ϕ_1 -direction have to be shown to show the behaviour of the effective potential.

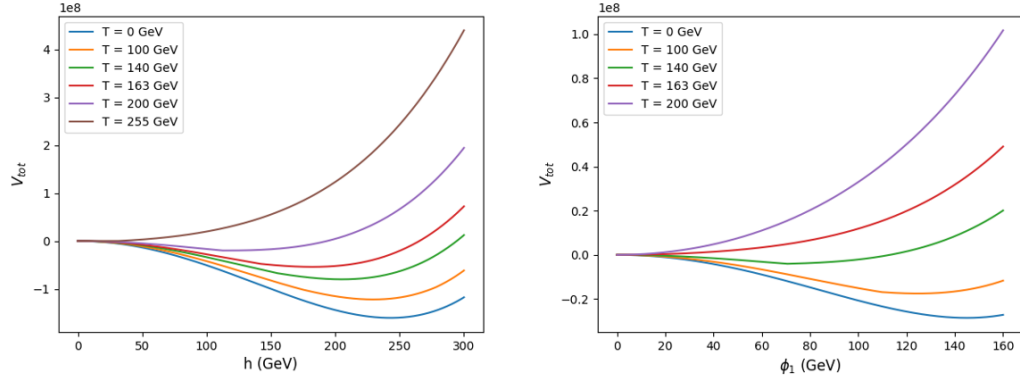


Figure 6.8: One-dimensional plots of the effective potential of the adjoint fSU(2)cSM for benchmark point 1 in Table 6.3. The plots are given at the VEV-values of the other fields.

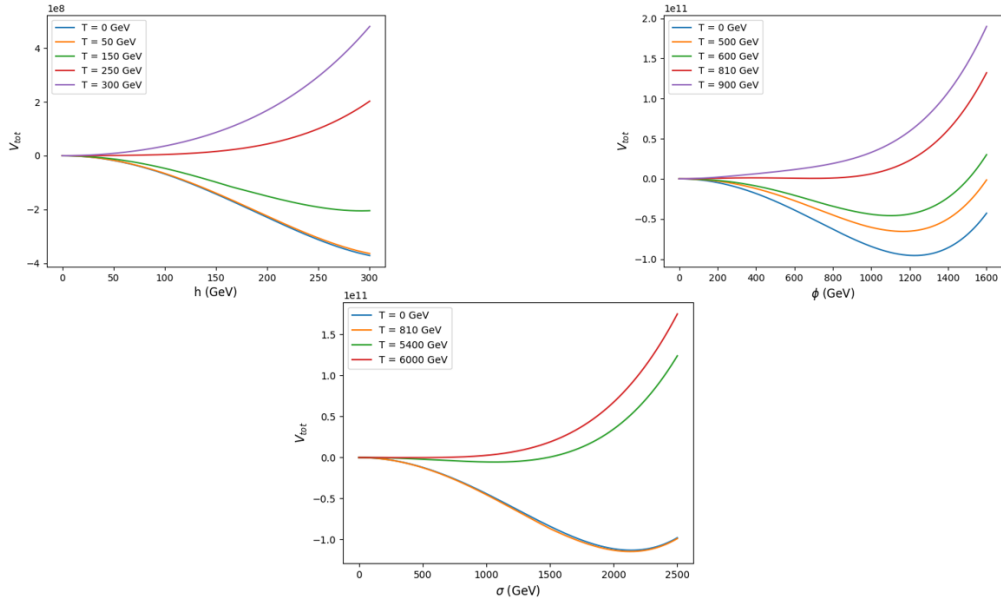


Figure 6.9: One-dimensional plots of the effective potential of the MfSU(2)cSM for benchmark point 1 in Table 6.4. The plots are given at the VEV-values of the other fields.

For the adjoint fSU(2)cSM the minimum becomes degenerate around 200 GeV. This is not completely clear from the ϕ_1 -figure in Figure 6.8, as the barrier is extremely small along the ϕ_1 - and ϕ_2 -direction. One can conclude from this two figures that there is likely a similar type of phase transition as for the SU(2)cSM model, where the scalar field tunnels along the $\phi_{1/2}$ -directions and then rolls down to the global minimum. It will therefore be of great interest to study the phase transitions in this model with Cos-

moTransitions.

The $MfSU(2)cSM$ gives a more complicated picture. All directions have a clear symmetry-breaking minimum for low temperatures, which disappears at high temperatures. However, the temperatures at which the minima are degenerate along a certain direction are very different for the three fields. Especially the σ -field already has a global symmetry-breaking minimum at temperatures around 6000 GeV. So this would indicate that tunneling would take place along the σ -direction. However, proper numerical tracking of the minima is needed to make sure that in the three-dimensional potential this is not a saddle point or the minimum is located elsewhere.

To conclude, CosmoTransitions is able to accurately track and describe the electroweak phase transition of $SU(2)cSM$. However, to do this, precise settings are needed for the numerical minimization procedures. As this could not be done in time for the adjoint $fSU(2)cSM$ and $MfSU(2)cSM$, this must be left for follow-up studies. However, one-dimensional analysis of the effective potentials clearly indicates interesting phase transitions, so these models are definitely of interest for a more extensive study.

Chapter 7

Conclusion

It is safe to state that conformal extensions of the Standard Model are one of the most promising theories of physics beyond the Standard Model. They are able to solve, or at least give an answer to, some of the most interesting open problems in Cosmology and particle physics. They can radiatively generate the Higgs mass and VEV, which otherwise is subject to an unnatural amount of fine-tuning. New particles in this conformal extension are also able to stabilize the Standard Model up to the Planck scale. Moreover, these particles can provide stable dark matter candidates and the extended scalar sector will undergo a first-order phase transition. This phase transition could not only accommodate baryogenesis, but in addition sources a gravitational wave background, which likely will be experimentally measurable in the near future.

These reasons were the original incentive to start on this study of conformal extensions of the Standard Model. To properly study these type of models, a theoretical framework of quantum and thermal field theory has been built in Chapter 2. With this framework, an effective potential can be constructed for any model, which includes quantum-loop and thermal-loop corrections. These corrections can induce a mass scale in the model through radiative symmetry breaking, whereas there was originally no mass scale. Furthermore, Daisy resummation has been discussed to control the perturbativity of the thermal field theory. General expressions were found for the scalar and gauge boson self-energies, which can be used for any model.

To narrow down the area of study, the possible theoretical and experimental constraints on conformal extensions were discussed in Chapter 3. It was concluded that one has to take into account what types of particles are added to any particular model, as they can be dark matter candidates or source baryogenesis. Furthermore, their interactions with the Higgs boson must be such that the SM values of the Higgs mass are retrieved.

In Chapter 4, old research on Grand Unified Theories has been reintroduced to give a feeling on the possible symmetry-breaking patterns of, in particular, $SU(N)$ and $SO(N)$ gauge groups. Again it was found that a general expression could be used, this time in the form of a mathematical conjecture. Next, three models were introduced. The first was the already studied $SU(2)$ cSM, which could be used in later chapters as a benchmark model. Then two new models were built with a diverse particle spectrum. The adjoint fSU(N)cSM is one of the few studied conformal extensions with a scalar sector in the adjoint representation. The other model, the MfSU(N)cSM, has multiple scalar interactions through three different scalars. Furthermore, it contains Majorana fermions, which could be of great interest for neutrino research. The complete mass spectra of all three models has been presented, where for the adjoint fSU(N)cSM, two different limits had to be considered to keep the expressions analytical.

Before it was possible to numerically analyze the three models, first a description of the electroweak phase transition was given in Chapter 5. As it turned out, it is possible to

generally describe the electroweak phase transition for conformal extensions. The transition is typically strong and first-order and is therefore able to source gravitational waves. To show this, the bubble nucleation and hydrodynamics have been studied and how the process of bubble collisions can produce gravitational waves. This has been implemented in the numerical program CosmoTransitions, which was introduced in Chapter 6. The results from the numerical analysis for the $SU(2)cSM$ were compared with previous results and were found to give a better description of the phase transition for this model. With the improved numerical calculations, several quantities were worked out. Finally, a plot of the expected stochastic gravitational wave background induced by the $SU(2)cSM$ was presented for all, but one, benchmark points. The peak frequencies were found to lie well within the expected sensitivity range of LISA.

Lastly, benchmark points were found for the adjoint $fSU(2)cSM$ and the $MfSU(2)cSM$. Unfortunately, the numerical analysis has not been able to work out before the completion of this thesis. A short description of the models, based on plots of the effective potential, was made and it could be concluded that the models behaved as expected. This means future work is needed for these models, but the framework built in this thesis, can be concluded to be solid.

To conclude, the questions asked in the introduction are still standing. From the work in this thesis, it is not yet possible to see if discrimination is possible between different models. Also, the influence of the particle spectra and the gauge groups on measurable quantities, such as the SGWB, are not yet studied. However, the thesis has been able to give guidelines to what is and what is not possible for conformal extension of the Standard Model. They can still provide answers to the problems left by the Standard Model, produce dark matter candidates and source baryogenesis. Different types of models can radiatively generate the Higgs mass and VEV and have electroweak symmetry breaking. So there is no need to constrain the research to the more minimalistic models as there has been found no indication that more complicated models are ruled out. In the contrary, the latter might be able to provide even more solutions. The future prospects are therefore encouraging for conformal extensions of the Standard Model and more research must and will be done on them. And in 15 years, perhaps a little longer, we might know for certain, whether one of these models is indeed the one that describes nature.

Appendix A

Full Lagrangian of the conformal extensions

For completeness, both full Lagrangians are given with clarification of the separate fields and terms. In both Lagrangians the Standard Model Lagrangian \mathcal{L}_{SM} is not written down explicitly and can be found in [105] for the Standard Model and for the conformal Standard Model in [13]. The fields G_i are the Goldstone bosons of the Standard Model, which form the pions after being eaten by the gauge bosons in the weak sector of the SM.

A.1 Lagrangian of the adjoint fSU(N)cSM

Model 1 consists of a dark matter sector with scalar fields, which transform in the adjoint representation under a $SU(N)$ gauge group. There are also Dirac fermions gauged under the same group.

$$\begin{aligned} \mathcal{L}_{model1} = & \mathcal{L}_{SM} + \lambda_1(H^\dagger H)^2 + \lambda_2(H^\dagger H) \text{Tr}[\Phi^\dagger \Phi] + \lambda_3 \text{Tr}[\Phi^\dagger \Phi]^2 + \lambda_4 \text{Tr}[(\Phi^\dagger \Phi)^2] \\ & + (D_\mu H)^\dagger D^\mu H + \text{Tr}[(D'_\mu \Phi)^\dagger D'^\mu \Phi] + \text{Tr}[G_{\mu\nu} G^{\mu\nu}] \end{aligned} \quad (\text{A.1})$$

$$+ i\bar{\psi} \not{D}' \psi + y_X \bar{\psi} \Phi \psi$$

$$H = \frac{1}{\sqrt{2}} \begin{pmatrix} G_2 + iG_3 \\ v + h + iG_1 \end{pmatrix} \quad (\text{A.2})$$

$$\Phi = \frac{1}{\sqrt{2}} \begin{pmatrix} \phi_1 & & \\ & \ddots & \\ & & \phi_N \end{pmatrix} \quad (\text{A.3})$$

$$\psi = \frac{1}{\sqrt{2}} (\psi_1, \dots, \psi_N)^T \quad (\text{A.4})$$

$$D'_\mu = \partial_\mu - ig_X X_\mu^a t_a \quad (\text{A.5})$$

Here t_a are the generators of the $SU(N)$ adjoint representation.

A.2 Lagrangian of the MfSU(N)cSM

The second model consists of three scalars of which two are in the dark sector. One is gauged in the fundamental representation of $SU(N)$, while the other is a complex scalar singlet. The singlet also interacts with un-gauged Majorana fermions.

$$\begin{aligned} \mathcal{L}_{model1} = & \mathcal{L}_{SM} + \lambda_1(H^\dagger H)^2 + \lambda_2(H^\dagger H)(\Phi^\dagger \Phi) + \lambda_3(\Phi^\dagger \Phi)^2 \\ & + \lambda_4(\Phi^\dagger \Phi)|\sigma|^2 + \lambda_5|\sigma|^4 \\ & + (D_\mu H)^\dagger D^\mu H + (D'_\mu \Phi)^\dagger D'^\mu \Phi + Tr[G_{\mu\nu}G^{\mu\nu}] \\ & + \frac{i}{2}\bar{\psi}\not{\partial}\psi + (\partial_\mu\sigma)^\dagger\partial_\mu\sigma + Y\sigma\bar{\psi}\psi + h.c. \end{aligned} \quad (\text{A.6})$$

$$H = \frac{1}{\sqrt{2}} \begin{pmatrix} G_2 + iG_3 \\ v + h + iG_1 \end{pmatrix} \quad (\text{A.7})$$

$$\Phi = \frac{1}{\sqrt{2}}(\phi_1 + \phi_2, \dots, \phi_{2N-1} + \phi_N)^T \quad (\text{A.8})$$

$$\psi = \frac{1}{\sqrt{2}}(\psi_1, \dots, \psi_{N_f})^T \quad (\text{A.9})$$

$$\sigma = \frac{1}{\sqrt{2}}(\sigma_1 + i\sigma_2) \quad (\text{A.10})$$

$$D'_\mu = \partial_\mu - ig_X X_\mu^a t_a \quad (\text{A.11})$$

The scalar fields are written in terms of real scalar fields h, G_i, ϕ_i and σ_i .

A.3 Thermal corrections to the Standard Model and the SU(2)cSM

The effective potential in the Standard Model was first calculated by Carrington in 1992 [36]. The contributions from Daisy resummation (he referred to the diagrams as ring diagrams) for the Standard Model particles are given below. As is explained in Section 2.3.2, only scalars and the longitudinal gauge bosons acquire a thermal mass at leading order.

The longitudinal masses in the gauge field basis (A_μ^a and B_μ) are given by:

$$M_L^2(h, T) = \frac{h^2}{4} \begin{pmatrix} g^2 & 0 & 0 & 0 \\ 0 & g^2 & 0 & 0 \\ 0 & 0 & g^2 & -gg' \\ 0 & 0 & -gg' & g'^2 \end{pmatrix} + \frac{11}{6}T^2 \begin{pmatrix} g^2 & 0 & 0 & 0 \\ 0 & g^2 & 0 & 0 \\ 0 & 0 & g^2 & 0 \\ 0 & 0 & 0 & g'^2 \end{pmatrix} \quad (\text{A.12})$$

Diagonalizing this matrix yields the familiar basis of the W_μ^\pm , Z_μ and photon γ [106]:

$$M_{W_L}^2(h, T) = m_W^2(h) + \frac{11}{6}g^2T^2 \quad (\text{A.13})$$

$$M_{Z_L}^2(h, T) = \frac{1}{2}m_Z^2(h) + \frac{11}{12}\frac{g^2}{\cos^2(\theta_W)}T^2 + \frac{\Delta}{2} \quad (\text{A.14})$$

$$M_{\gamma_L}^2(h, T) = \frac{1}{2}m_Z^2(h) + \frac{11}{12}\frac{g^2}{\cos^2(\theta_W)}T^2 - \frac{\Delta}{2} \quad (\text{A.15})$$

$$\Delta^2 = m_Z^4(h) + \frac{11}{3}\frac{g^2 \cos^2(2\theta_W)}{\cos^2(\theta_W)} \left[m_z^2(h) + \frac{11}{12}\frac{g^2}{\cos^2(\theta_W)}T^2 \right] T^2 \quad (\text{A.16})$$

The gauge bosons in the SU(2)cSM have a mass similar to the W_μ -bosons. Ideally, one would like to include a transition function between the thermal mass and the tree-level mass [15]. This is due to the fact that the high temperature limit is not valid for field

A.3. THERMAL CORRECTIONS TO THE STANDARD MODEL AND THE $SU(2)$ CSM59

values around the VEV where the found tree-level mass is $m_X \sim \mathcal{O}(1 \text{ TeV})$ at GeV-scales of temperature. Here one rather uses the tree-level mass. However, it was found that including a tanh-like transition function, would force the local minimum away from the origin.

$$M_{X_L}(\phi, T) = m_X^2(\phi) + \frac{5}{6}g_X^2 T^2 \quad (\text{A.17})$$

Appendix B

HTL calculation of the scalar self-energy

The one-loop scalar self-energy is the most simple to determine. It can have contributions from loop diagrams with scalar-, fermion- and gauge-loops, as shown in Figure B.1. This is for a Higgs-like scalar particle with general gauge and fermion interactions. For conformal extensions, interactions with other scalars are also possible, but they can be simply derived from the different multiplicity of the scalar loop diagram.

To do the calculations, one needs the different type of propagators and some standard integral identities from TFT. They are given in Feynmann gauge for a general metric $g_{\mu\nu}$ and K is the four-vector momentum $K = (k_0, \vec{k})$. Note that the scalar and fermion propagator seem similar, but differ in the allowed Matsubara frequencies $\omega_n = (2n+1)\pi T$ for fermions.

$$\text{Scalar/fermion propagator: } \Delta(K) = \frac{1}{K^2 - \Pi(k_0, \vec{k})} \quad (\text{B.1})$$

$$\text{Gauge propagator: } \Delta_{\mu\nu}^{ab}(K) = g_{\mu\nu} \delta^{ab} \Delta(K) \quad (\text{B.2})$$

$$T \sum_{k_0} \int \frac{d^3 k}{(2\pi)^3} \Delta(K) = \frac{T^2}{12} \quad (\text{B.3})$$

Equation (B.3) can be easily derived using a complex contour integral for the sum and then changing to spherical coordinates for the spatial integrals. Now everything is given to calculate the scalar self-energy to one-loop order. The contributing diagrams are shown in Figure B.1.

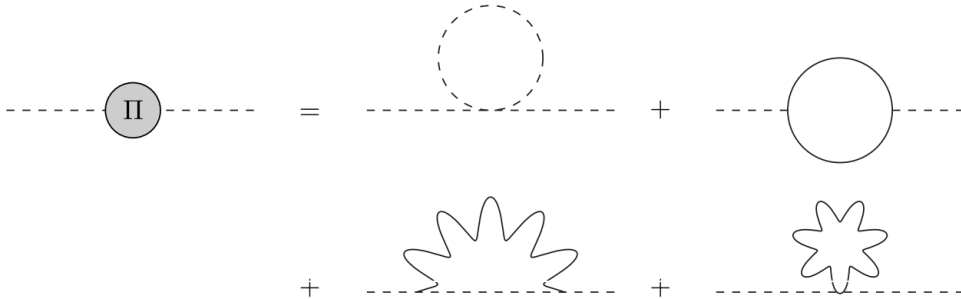


Figure B.1: Possible contributing diagrams to the one-loop scalar self-energy Π . The diagrams have scalar-, fermion- and gauge-loops, respectively. Picture taken from [42].

First, the scalar loop is considered. Here a Higgs-like scalar is assumed, which is a $SU(2)$ doublet. Counting the number of possible Wick contractions gives a multiplicity

of 6, however for any other scalar or a loop diagram with interactions between different scalars this number can differ. So the vertex factor is 6λ , where λ is the self-interaction coupling. Then the self-energy contribution from this loop-diagram is given by:

$$\Pi_\phi = 6\lambda T \sum_{k_0} \int \frac{d^3k}{(2\pi)^3} \Delta(K) = \frac{\lambda T^2}{2} \quad (\text{B.4})$$

The typical gauge contribution comes from two diagrams. The gauge coupling is here denoted by g , t^a are the generators of the gauge group and Q is the external momentum. This yields the following contribution:

$$\Pi_{\text{gauge}} = g^2 t^a t^b T \sum_{k_0} \int \frac{d^3k}{(2\pi)^3} \left[(2Q - K)^\mu \Delta_{\mu\nu}^{ab}(K) (2Q - K)^\nu \Delta(Q - K) + \frac{1}{2} (-2g^{\mu\nu}) \Delta_{\mu\nu}^{ab}(K) \right] \quad (\text{B.5})$$

where the factor $\frac{1}{2}$ is a symmetry factor of the second loop diagram. Now one uses $t^a t^b \delta_{ab} = C_2(r)$ with $C_2(r)$ the Casimir-invariant of the gauge group in representation r . Also assuming soft external momentum, one can approximate $(2Q - K)^2 \approx K^2$. Then by shifting the loop momentum $K \rightarrow Q - K$ for the second diagram, the dependence on the external momentum Q is completely eliminated:

$$\begin{aligned} \Pi_{\text{gauge}} &= g^2 C_2(r) T \sum_{k_0} \int \frac{d^3k}{(2\pi)^3} [4\Delta(K) - \Delta(K)] \\ &= \frac{g^2 C_2(r) T^2}{4} \end{aligned} \quad (\text{B.6})$$

Lastly, the fermion loop-diagram is calculated. The vertex factor depends on the number of colours and is thus generally given by $N_c \lambda_f$. This gives the self-energy:

$$\Pi_f = -N_c \lambda_f^2 T \sum_{k_0} \int \frac{d^3k}{(2\pi)^3} \text{Tr}[P_L \not{K} (\not{K} - \not{Q})] \Delta(K) \Delta(K - Q) \quad (\text{B.7})$$

where a minus sign is added for the fermion loop. The trace is equal to:

$$\text{Tr}[P_L \not{K} (\not{K} - \not{Q})] = 2K \cdot (K - Q) = K^2 + (K - Q)^2 - Q^2 \quad (\text{B.8})$$

As the external momentum is assumed to be soft, contributions of Q^2 can be neglected. This yields:

$$\Pi_f = -N_c \lambda_f^2 T \sum_{k_0} \int \frac{d^3k}{(2\pi)^3} [\Delta(K) + \Delta(K - Q)] \quad (\text{B.9})$$

The identity in Equation (B.3) differs a factor of $-\frac{1}{2}$ for the fermion propagator due to the different Matsubara poles in the complex contour integral. Again shifting the momentum in the second term yields the final expression:

$$\Pi_f = \frac{N_c \lambda_f^2 T^2}{12} \quad (\text{B.10})$$

Putting all terms together, gives a general expression for the self-energy of a Higgs-like scalar:

$$m_{\phi, \text{thermal}}^2 = \frac{6\lambda + 3g^2 C_2(r) + N_c \lambda_f^2 T^2}{12} \quad (\text{B.11})$$

Again, note that for different models the multiplicity factors will differ.

Appendix C

Explicit expressions for the symmetry breaking analysis

Here the explicit expressions for the terms $a(n_1, n_2, n_3)$, $(n_1, n_2, n_3)b$ and $f(n_1, n_2, n_3)$ are given, as introduced in Section 4.1.2. The terms are for symmetry breaking of a second-rank symmetric tensor in the $O(N)$ group. The analysis can also be found in appendix B of [72]. The terms are given by:

$$a(n_1, n_2, n_3) = \frac{\mu^2}{2} \frac{1}{(n_2 - n_3)^2} [n_1(n_2 - n_3)^2 + n_2(n_1 - n_3)^2 + n_3(n_1 - n_2)^2] \quad (\text{C.1})$$

$$b(n_1, n_2, n_3) = \frac{1}{4(n_2 - n_3)^4} [\lambda_1 (n_1(n_2 - n_3)^2 + n_2(n_1 - n_3)^2 + n_3(n_1 - n_2)^2) + \lambda_2 (n_1(n_2 - n_3)^4 + n_2(n_1 - n_3)^4 + n_3(n_1 - n_2)^4)] \quad (\text{C.2})$$

$$f(n_1, n_2, n_3) = \frac{n_1(n_2 - n_3)^4 + n_2(n_1 - n_3)^4 + n_3(n_1 - n_2)^4}{[n_1(n_2 - n_3)^2 + n_2(n_1 - n_3)^2 + n_3(n_1 - n_2)^2]^2} \quad (\text{C.3})$$

Bibliography

- [1] S. Furlanetto et al., *Astro 2020 Science White Paper: Fundamental Cosmology in the Dark Ages with 21-cm Line Fluctuations*, [arXiv:1903.06212](#).
- [2] ATLAS and CMS Collaborations, *Combined Measurement of the Higgs Boson Mass in pp collisions at $\sqrt{s}=7$ and 8 TeV with the ATLAS and CMS Experiments*, [arXiv:1503.07589](#).
- [3] ATLAS Collaboration, *Measurements of Higgs boson production and couplings in the four-lepton channel in pp collisions at center-of-mass energies of 7 and 8 TeV with the ATLAS detector*, [arXiv:1408.5191](#).
- [4] CMS Collaboration, *Precise determination of the mass of the Higgs boson and tests of compatibility of its couplings with the standard model predictions using proton collisions at 7 and 8 TeV*, [arXiv:1412.8662](#).
- [5] F. Englert and R. Brout, *Broken Symmetry and the Mass of Gauge Vector Mesons*, *Physical Review Letters* **13** (8, 1964) 321–323.
- [6] P. W. Higgs, *Broken Symmetries and the Masses of Gauge Bosons*, *Physical Review Letters* **13** (10, 1964) 508–509.
- [7] W. A. Bardeen, *On naturalness in the standard model*, in *Ontake Summer Institute on Particle Physics Ontake Mountain, Japan, August 27-September 2, 1995*, 1995.
- [8] P. Draper, P. Meade, M. Reece, and D. Shih, *Implications of a 125 GeV Higgs boson for the MSSM and low-scale supersymmetry breaking*, *Physical Review D* **85** (5, 2012) 095007.
- [9] S. Coleman and E. Weinberg, *Radiative corrections as the origin of spontaneous symmetry breaking*, *Physical Review D* **7** (1973), no. 6 1888–1910, [[hep-th/0507214](#)].
- [10] L. Chataignier, T. Prokopec, M. G. Schmidt, and B. Świeżewska, *Systematic analysis of radiative symmetry breaking in models with extended scalar sector*, *Journal of High Energy Physics* **2018** (2018), no. 8 [[arXiv:1805.09292](#)].
- [11] Y. Tang, *Vacuum Stability in the Standard Model*, [arXiv:1301.5812v](#).
- [12] A. Beniwal, M. Lewicki, M. White, and A. G. Williams, *A global study of the extended scalar singlet model*, [arXiv:1809.01686](#).
- [13] K. A. Meissner and H. Nicolai, *Conformal Symmetry and the Standard Model*, [hep-th/0612165](#).
- [14] A. Karam and K. Tamvakis, *Dark matter and neutrino masses from a classically scale-invariant multi-Higgs portal*, in *Proceedings of Science*, 8, 2015. [arXiv:1508.03031](#).
- [15] T. Prokopec, J. Rezacek, and B. Świeżewska, *Gravitational waves from conformal symmetry breaking*, [arXiv:1809.11129](#).

- [16] S. Di Chiara and K. Tuominen, *A minimal model for $SU(N)$ vector dark matter*, *Journal of High Energy Physics* **2015** (2015), no. 11 1–15, [arXiv:1506.03285].
- [17] I. Baldes and C. Garcia-Cely, *Strong gravitational radiation from a simple dark matter model*, *JHEP* **05** (2019) 190, [arXiv:1809.01198].
- [18] D. Croon, V. Sanz, and G. White, *Model Discrimination in Gravitational Wave spectra from Dark Phase Transitions*, arXiv:1806.02332.
- [19] Y. Wan, B. Imtiaz, and Y.-F. Cai, *Cosmological phase transitions and gravitational waves in the singlet Majoron model*, arXiv:1804.05835.
- [20] F. Antonuccio and S. S. Pinsky, *Matrix theories from reduced $SU(N)$ Yang-Mills with adjoint fermions*, *Physics Letters B* **397** (3, 1997) 42–50.
- [21] D. Kirzhnits and A. Linde, *Macroscopic consequences of the Weinberg model*, *Physics Letters B* **42** (12, 1972) 471–474.
- [22] Kirzhnits D.A., *Weinberg Model and the ‘Hot’ Universe*, *JETP Letters* **15** (1972), no. 12 529.
- [23] G. W. Anderson and L. J. Hall, *The Electroweak phase transition and baryogenesis*, *Phys. Rev.* **D45** (1992) 2685–2698.
- [24] P. Amaro-Seoane et al., *Laser Interferometer Space Antenna*, *arXiv e-prints* (Feb, 2017) arXiv:1702.00786, [arXiv:1702.00786].
- [25] N. J. Cornish, E. Berti, K. Holley-Bockelmann, S. Larson, S. McWilliams, G. Mueller, P. Natarajan, and M. Vallisneri, *The Discovery Potential of Space-Based Gravitational Wave Astronomy*, arXiv:1904.01438.
- [26] S. T. McWilliams, R. Caldwell, K. Holley-Bockelmann, S. L. Larson, and M. Vallisneri, *Astro2020 Decadal Science White Paper: The state of gravitational-wave astrophysics in 2020*, arXiv:1903.04592.
- [27] R. Caldwell, M. Amin, C. Hogan, K. Holley-Bockelmann, D. Holz, P. Jetzer, E. Kovetz, P. Natarajan, D. Shoemaker, T. Smith, and N. Tamanini, *Astro2020 Science White Paper: Cosmology with a Space-Based Gravitational Wave Observatory*, arXiv:1903.04657.
- [28] L. Chataignier, *Radiative Symmetry Breaking in Classically Conformal Extensions of the Standard Model*, .
- [29] J. Rezaeck, *Cosmological Phase Transitions and Conformal Extensions of the Standard Gravitational Wave Production in Model*. PhD thesis, Utrecht University, 2018.
- [30] C. L. Wainwright, *CosmoTransitions: Computing Cosmological Phase Transition Temperatures and Bubble Profiles with Multiple Fields*, arXiv:1109.4189.
- [31] J. Goldstone, A. Salam, and S. Weinberg, *Broken Symmetries*, *Physical Review* **127** (8, 1962) 965–970.
- [32] R. Jackiw, *Functional evaluation of the effective potential*, *Physical Review D* **9** (3, 1974) 1686–1701.
- [33] A. Salam and J. C. Ward, *Weak and electromagnetic interactions*, *Il Nuovo Cimento* **11** (2, 1959) 568–577.
- [34] S. L. Glashow, *The renormalizability of vector meson interactions*, *Nuclear Physics* **10** (2, 1959) 107–117.
- [35] S. Weinberg, *A Model of Leptons*, *Physical Review Letters* **19** (11, 1967) 1264–1266.

- [36] M. E. Carrington, *The Effective potential at finite temperature in the Standard Model*, *Phys. Rev.* **D45** (1992) 2933–2944.
- [37] M. Le Bellac, *Thermal Field Theory*. Cambridge University Press, Cambridge, 1996.
- [38] M. Laine and A. Vuorinen, *Basics of Thermal Field Theory*, vol. 925. Springer Lecture Notes, 1, 2016.
- [39] T. Altherr, *Introduction to Thermal Field Theory*, *International Journal of Modern Physics A* **08** (7, 1993) 5605–5628, [[hep-ph/9307277](#)].
- [40] M. Laine and K. Rummukainen, *What’s new with the electroweak phase transition?*, [hep-lat/9809045](#).
- [41] P. B. Arnold and O. Espinosa, *The Effective potential and first order phase transitions: Beyond leading-order*, *Phys. Rev.* **D47** (1993) 3546, [[hep-ph/9212235](#)]. [Erratum: *Phys. Rev.*D50,6662(1994)].
- [42] D. Besak, *Thermal particle production in the early Universe*. PhD thesis, Bielefeld University, 2010.
- [43] J. R. Espinosa, M. Quiros, and F. Zwirner, *On the phase transition in the scalar theory*, *Phys. Lett.* **B291** (1992) 115–124, [[hep-ph/9206227](#)].
- [44] R. D. Pisarski, *Computing Finite Temperature Loops with Ease*, *Nucl. Phys.* **B309** (1988) 476–492.
- [45] T. Matsubara, *A New Approach to Quantum-Statistical Mechanics*, *Progress of Theoretical Physics* **14** (10, 1955) 351–378.
- [46] E. J. Weinberg and A. Wu, *Understanding complex perturbative effective potentials*, *Physical Review D* **36** (10, 1987) 2474–2480.
- [47] L. Dolan and R. Jackiw, *Symmetry behavior at finite temperature*, *Physical Review D* **9** (6, 1974) 3320–3341.
- [48] M. Dine, R. G. Leigh, P. Huet, A. D. Linde, and D. A. Linde, *Comments on the Electroweak Phase Transition*, [hep-ph/9203201](#).
- [49] R. R. Parwani, *Resummation in a Hot Scalar Field Theory*, .
- [50] E. Braaten and R. D. Pisarski, *Soft amplitudes in hot gauge theories: A general analysis*, *Nuclear Physics B* **337** (6, 1990) 569–634.
- [51] S. Weinberg, *Cosmology*. Oxford University Press, 2008.
- [52] E. W. Kolb and M. S. Turner, *The early universe*, vol. 69. Westview Press, 1994.
- [53] P. Collaboration, *Planck 2018 results. VI. Cosmological parameters*, [arXiv:1807.06209](#).
- [54] Planck Collaboration, *Planck 2015 results. XIII. Cosmological parameters*, [arXiv:1502.01589](#).
- [55] E. Komatsu et al., *Seven-Year Wilkinson Microwave Anisotropy Probe (WMAP) Observations: Cosmological Interpretation*, [arXiv:1001.4538](#).
- [56] W. Bernreuther, *CP violation and baryogenesis*, [hep-ph/0205279](#).
- [57] A. D. Sakharov, *Violation of CP in variance, C asymmetry, and baryon asymmetry of the universe*, *JETP Lett.* **5** (5, 1967) 24–27.
- [58] J. de Vries, M. Postma, J. van de Vis, and G. White, *Electroweak baryogenesis and the standard model effective field theory*, *Journal of High Energy Physics* **2018** (1, 2018) 89.

- [59] V. Kuzmin, V. Rubakov, and M. Shaposhnikov, *On anomalous electroweak baryon-number non-conservation in the early universe*, *Physics Letters B* **155** (5, 1985) 36–42.
- [60] P. Kooijman and N. Tuning, “Lectures on CP violation.” <https://www.nikhef.nl/~h71/Lectures/2015/ppII-cpviolation-29012015.pdf>, 2015. Online; accessed 24 February 2019.
- [61] A. Hocker and Z. Ligeti, *CP violation and the CKM matrix*, [hep-ph/0605217](https://arxiv.org/abs/hep-ph/0605217).
- [62] K. Kannike, *Vacuum Stability Conditions From Copositivity Criteria*, [arXiv:1205.3781](https://arxiv.org/abs/1205.3781).
- [63] J. Chakraborty, P. Konar, and T. Mondal, *Copositive Criteria and Boundedness of the Scalar Potential*, [arXiv:1311.5666](https://arxiv.org/abs/1311.5666).
- [64] T. Hambye and A. Strumia, *Dynamical generation of the weak and Dark Matter scale*, [arXiv:1306.2329](https://arxiv.org/abs/1306.2329).
- [65] C. Gross, O. Lebedev, and Y. Mambrini, *Non-Abelian gauge fields as dark matter*, [arXiv:1505.07480](https://arxiv.org/abs/1505.07480).
- [66] M. Luo, H. Wang, and Y. Xiao, *Two-loop Renormalization Group Equations in General Gauge Field Theories*, [hep-ph/0211440](https://arxiv.org/abs/hep-ph/0211440).
- [67] L. Michel and L. A. Radicati, *Properties of the breaking of hadronic internal symmetry*, *Annals of Physics* **66** (8, 1971) 758–783.
- [68] J. S. Kim, *General method for analyzing Higgs potentials*, *Nuclear Physics B* **196** (3, 1982) 285–300.
- [69] J. S. Kim, *SO(N) higgs problem with adjoint+vector representations and non-linear potentials*, *Nuclear Physics B* **207** (11, 1982) 374–398.
- [70] J. Sam Kim, *SU(N) Higgs problem with adjoint representation and Michel’s conjecture*, *Nuclear Physics* **197** (1982) 174–188.
- [71] H. Ruegg, *Extrema of SU(n) higgs potentials and symmetry-breaking pattern*, *Phys. Rev. D* **22** (Oct, 1980) 2040–2044.
- [72] L.-F. Li, *Group theory of the spontaneously broken gauge symmetries*, *Physical Review D* **9** (3, 1974) 1723–1739.
- [73] V. Elias, S. Eliezer, and A. R. Swift, *Comment on “Group theory of the spontaneously broken gauge symmetries”*, *Physical Review D* **12** (1975), no. 10 3356.
- [74] K. K. Boddy, J. L. Feng, M. Kaplinghat, and T. M. P. Tait, *Self-interacting dark matter from a non-Abelian hidden sector*, [arXiv:1402.3629v](https://arxiv.org/abs/1402.3629v).
- [75] W. Ochs, *The Status of Glueballs*, [arXiv:1301.5183](https://arxiv.org/abs/1301.5183).
- [76] O. Lebedev, H. M. Lee, and Y. Mambrini, *Vector Higgs-portal dark matter and the invisible Higgs*, [arXiv:1111.4482](https://arxiv.org/abs/1111.4482).
- [77] L. Ackerman, M. R. Buckley, S. M. Carroll, and M. Kamionkowski, *Dark Matter and Dark Radiation*, [arXiv:0810.5126](https://arxiv.org/abs/0810.5126).
- [78] Y. Cui, M. Lewicki, D. E. Morrissey, and J. D. Wells, *Probing the pre-BBN universe with gravitational waves from cosmic strings*, [arXiv:1808.08968](https://arxiv.org/abs/1808.08968).
- [79] V. V. Khoze, C. McCabe, and G. Ro, *Higgs vacuum stability from the dark matter portal*, [arXiv:1403.4953](https://arxiv.org/abs/1403.4953).

- [80] F. Loebbert, J. Miczajka, and J. Plefka, *Consistent Conformal Extensions of the Standard Model*, [arXiv:1805.09727](https://arxiv.org/abs/1805.09727).
- [81] C. D. Carone and R. Ramos, *Classical scale-invariance, the electroweak scale and vector dark matter*, [arXiv:1307.8428](https://arxiv.org/abs/1307.8428).
- [82] G. 't Hooft, *A planar diagram theory for strong interactions*, *Nuclear Physics B* **72** (4, 1974) 461–473.
- [83] M. Gabella, *Non-Abelian Gauge Theories with Spontaneous Symmetry Breaking : Higgs Mechanism*, .
- [84] H. E. Haber, “Useful relations among the generators in the defining and adjoint representations of $SU(N)$.” <https://pdfs.semanticscholar.org/1101/914fc76a36d4fb0ab0022f8c4ec6295d8d1f.pdf>. Online; accessed 12 January 2019.
- [85] L. Wantzel, *Classification des nombres incommensurables d’origine algébrique*, *Nouvelles annales de mathématiques : journal des candidats aux écoles polytechnique et normale* **1e série**, **2** (1843) 117–127.
- [86] O. K. Smith and O. K., *Eigenvalues of a symmetric 3 x 3 matrix*, *Communications of the ACM* **4** (4, 1961) 168.
- [87] M. Gell-Mann, R. Slansky, and P. Ramond, *Complex Spinors and Unified Theories*, *Conf.Proc.* **C790927** (1979) 315–321.
- [88] T. Yanagida, *Horizontal Symmetry and Masses of Neutrinos*, *Progress of Theoretical Physics* **64** (9, 1980) 1103–1105.
- [89] K. S. Babu, I. Gogoladze, and S. Khan, *Radiative Electroweak Symmetry Breaking in Standard Model Extensions*, [arXiv:1612.05185](https://arxiv.org/abs/1612.05185).
- [90] D. Cogollo, R. D. Matheus, T. B. de Melo, and F. S. Queiroz, *Type I + II Seesaw in a Two Higgs Doublet Model*, [arXiv:1904.07883](https://arxiv.org/abs/1904.07883).
- [91] J. Ellis, M. Lewicki, J. M. No, and V. Vaskonen, *Gravitational wave energy budget in strongly supercooled phase transitions*, [arXiv:1903.09642](https://arxiv.org/abs/1903.09642).
- [92] A. Linde, *Decay of the false vacuum at finite temperature*, *Nuclear Physics B* **216** (5, 1983) 421–445.
- [93] J. Ellis, M. Lewicki, and J. M. No, *On the Maximal Strength of a First-Order Electroweak Phase Transition and its Gravitational Wave Signal*, [arXiv:1809.08242](https://arxiv.org/abs/1809.08242).
- [94] V. K. Shante and S. Kirkpatrick, *An introduction to percolation theory*, *Advances in Physics* **20** (5, 1971) 325–357.
- [95] T. Konstandin and G. Servant, *Cosmological Consequences of Nearly Conformal Dynamics at the TeV scale*, [arXiv:1104.4791](https://arxiv.org/abs/1104.4791).
- [96] C. Caprini, M. Hindmarsh, S. Huber, T. Konstandin, J. Kozaczuk, G. Nardini, J. M. No, A. Petiteau, P. Schwaller, G. Servant, and D. J. Weir, *Science with the space-based interferometer eLISA. II: Gravitational waves from cosmological phase transitions*, [arXiv:1512.06239](https://arxiv.org/abs/1512.06239).
- [97] D. Bodeker and G. D. Moore, *Electroweak Bubble Wall Speed Limit*, [arXiv:1703.08215](https://arxiv.org/abs/1703.08215).
- [98] M. Hindmarsh, S. J. Huber, K. Rummukainen, and D. J. Weir, *Numerical simulations of acoustically generated gravitational waves at a first order phase transition*, [arXiv:1504.03291](https://arxiv.org/abs/1504.03291).

- [99] P. Athron, C. Balázs, M. Bardsley, A. Fowlie, D. Harries, and G. White, *Bubbleprofiler: finding the field profile and action for cosmological phase transitions*, [arXiv:1901.03714](#).
- [100] A. Masoumi, K. D. Olum, and J. M. Wachter, *Approximating tunneling rates in multi-dimensional field spaces*, [arXiv:1702.00356](#).
- [101] P. Basler and M. Muhlleitner, *BSMPT - Beyond the Standard Model Phase Transitions - A Tool for the Electroweak Phase Transition in Extended Higgs Sectors*, [arXiv:1803.02846](#).
- [102] A. Fowlie, *A fast C++ implementation of thermal functions*, [arXiv:1802.02720](#).
- [103] T. Robson, N. Cornish, and C. Liu, *The construction and use of LISA sensitivity curves*, [arXiv:1803.01944](#).
- [104] C. J. Moore, R. H. Cole, and C. P. L. Berry, *Gravitational-wave sensitivity curves*, [arXiv:1408.0740](#).
- [105] P. Langacker, *Structure of the Standard Model*, [hep-ph/0304186](#).
- [106] L. D. Rose, C. Marzo, and A. Urbano, *On the fate of the Standard Model at finite temperature*, [arXiv:1507.06912](#).